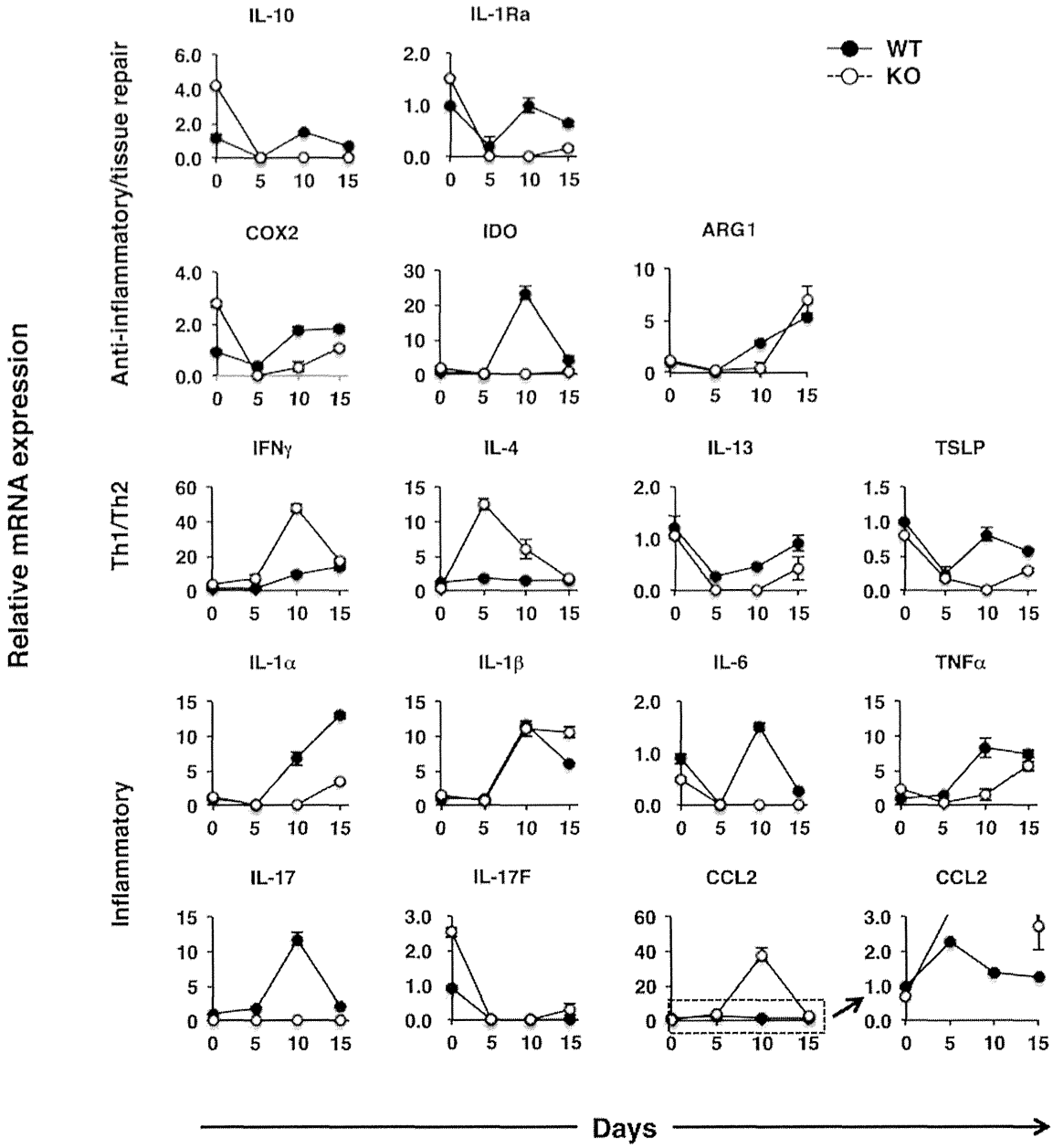

Figure 2. Colonic expression of mRNA for genes involved in inflammation and anti-inflammation. IL-17KO mice and WT controls were treated with DSS as described in the legend for Figure 1. Total RNA were purified from distal colon sections of untreated and DSS-treated individual mice (n = 3) and transcribed into cDNA, which were subsequently subjected for real-time PCR analysis. Expression of target mRNA were normalized to the expression of β-actin mRNA for generation of ΔCt values, and relative mRNA expression was quantified with the ΔΔCt method. Data are expressed as mean ± SEM. *$p<0.05$; **$p<0.01$.
doi:10.1371/journal.pone.0108494.g002

more severely compromised by DSS administration than that in WT mice as IL-17KO mice displaying a dramatic increase in orally administered FITC-dextran translocation into the serum (Figure 1D). Although WT mice treated with DSS did not exhibit overt symptoms of progressive wasting disease, we observed an increased number of inflammatory infiltrates and IL-17$^+$ cells in the colon of WT mice treated with DSS as compared to the colons of untreated WT mice (Figure 1C and data not shown).

Inflamed colons of IL-17KO mice expressed reduced levels of mRNA with anti-inflammatory functions

Using real-time PCR samples taken from the colons of WT and IL-17KO mice, we next assessed the expression of mRNA for a range of genes thought to be involved in inflammatory/anti-inflammatory responses. mRNA for IL-10, IL-1 receptor antagonist (IL-1Ra), arginase 1 (ARG1), cyclooxygenase 2 (COX2), and indoleamine 2,3-dioxygenase (IDO), which are produced by M2 and/or wound healing macrophages contributing to the suppres-

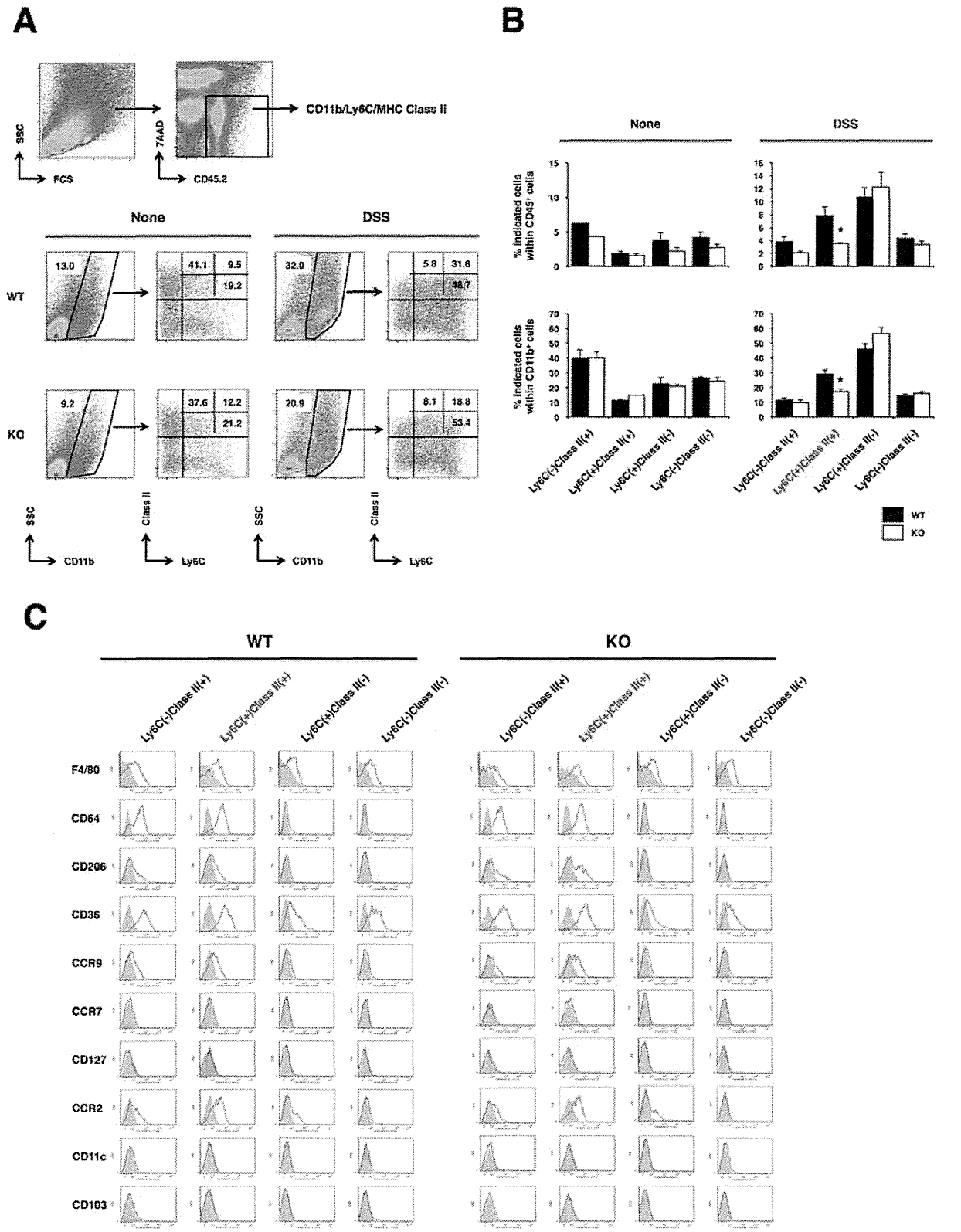

Figure 3. Aggravated DSS-induced colitis in IL-17KO mice is associated with reduced number of CD11b$^+$Ly6C$^+$MHC Class II$^+$ macrophages in the inflamed colon. IL-17KO mice and WT controls were treated with DSS as described in the legend for Figure 1. (A) LPLs were purified from pooled (n = 2–3) distal colon sections of untreated and DSS-treated mice and subjected to flow cytometry analysis. Gating strategy of

live and CD45$^+$ for CD11b$^+$ cells was shown in upper panels. Representative data from seven independent experiments are shown. Number denotes frequency of gated cells. (B) The frequency of cells for each subset in A is shown. Graphs represent mean ± SEM of seven independent experiments. *$p<0.05$. (C) Representative flow cytometry profiles of cell surface molecules implicated in M2/anti-inflammatory macrophages on each subset depicted as in A. Gray histograms represent cells stained with isotype matched control mAbs.
doi:10.1371/journal.pone.0108494.g003

sion/resolution of inflammation and tissue repair [20], were significantly reduced in IL-17KO mice at the peak of colon inflammation (day 10), as compared to WT mice (Figure 2). Notably, among mRNA for IL-22, DARC, and D6, all of which also have tissue repair and anti-inflammatory functions and are produced by a variety of cell types other than macrophages [21,22], only DARC mRNA was significantly reduced in IL-17KO mice (data not shown). As for expression levels of Th1 and Th2 signature cytokines, the expression of IFN-γ and IL-4 mRNA were significantly upregulated in IL-17KO mice with severe colitis. Those for other inflammatory cytokines, such as IL-1α, IL-1β, and TNFα, were increased in the colon of both WT and IL-17KO mice after DSS treatment. However, somewhat unexpectedly, expression levels of IL-1α and TNFα were lower in the colons of IL-17KO mice. Moreover, IL-6 mRNA was upregulated only in inflamed colons of WT mice. The expression level of mRNA for IL-17, but not its related cytokine IL-17F, was increased in colon of WT mice after DSS treatment.

Aggravated colitis seen in IL-17KO mice correlates with the lack of CD11b$^+$Ly6c$^+$MHC Class II$^+$ macrophages

Intestinal macrophages are highly versatile in function and can suppress inflammation and/or promote repair of damaged mucosal tissues [23]. Together with our results that genes involved in anti-inflammatory/tissue repair, which expressed in M2/wound healing macrophages were reduced in the inflamed colon of IL-17KO mice mentioned above, led us to examine for differences between macrophage subpopulations in the inflamed colon of WT and IL-17KO mice. As an initial step, we performed multi-color flow cytometric analysis for mononuclear cells of colonic lamina propria taken from IL-17KO and WT mice before and after induction of colitis. At a steady state, there is only a small difference in the proportion of CD11b$^+$ cells, and subsets within CD11b$^+$ cell population of colonic lamina propria leukocytes (LPLs) from IL-17KO and WT mice (Figure 3A and B). Inflamed colonic LPLs contained an increasing trend in the proportion of CD11b$^+$ cell infiltrates but this increase was less prominent in IL-17KO mice (Figure 3A). On the other hand, there was a significant difference in the proportion of Ly6C$^+$MHC Class II$^+$ cells between WT and IL-17KO mice within CD11b$^+$ cell population (Figure 3B). Inflamed colonic LPLs of IL-17KO mice contained a significantly lower proportion of Ly6C$^+$MHC Class II$^+$ cells. As for other cell types involved in the regulation of mucosal immune responses, there was a notable decrease in frequency of CD4$^+$Foxp3$^+$ regulatory T cells in the inflamed colon LPLs of IL-17KO mice (Figure S1). We then looked at expression levels of CD206, CD36 and CCR9 along with F4/80 and CD64, all of which are associated with macrophages bearing anti-inflammatory and/or tissue repair function [20,23,24], on individual subpopulations as defined by Ly6C and MHC Class II within CD11b$^+$ cells (Figure 3C). Ly6C$^+$MHC Class II$^+$ and Ly6C$^-$MHC Class II$^+$ subpopulations expressed higher levels of those molecules as compared to Ly6C$^+$MHC Class II$^-$ and Ly6C$^-$MHC Class II$^-$ subpopulations in inflamed colonic LPLs of WT and IL-17KO mice. Consistent with these findings, immunohistochemical analysis of colonic tissue sections showed that the inflamed colons of WT mice enriched Ly6C$^+$MHC Class II$^+$ and Ly6C$^+$CD206$^+$ cells, but these features were less prominent in IL-17KO mice (data not shown). As for cell surface markers, such as CCR7, CD127, CD11c, and CD103 implicated in M1 macrophages and dendritic cells, both of which have been shown to play proinflammatory role in colitis [20,23,25] were not expressed on either subpopulations within CD11b$^+$ cells (Figure 3C).

CD11b$^+$ cells in the inflamed colonic LPLs of WT mice express signature transcription factors and their target genes implicated in anti-inflammatory M2/wound healing macrophages

To gain insight into the unique features of macrophages that emerged in the inflamed colons of WT that seem to have regulatory function for colitis, we looked into genes expressed in CD11b$^+$ cells, more abundant in Ly6C$^+$MHC Class II$^+$ cell in LP of colitic WT mice as compared to those from IL-17KO mice. To this end, CD11b$^+$ cells from LP of colitic WT and IL-17KO mice were purified by FACS (Figure S2), and their mRNAs were subjected to real-time PCR analysis. As shown in Figure 4A, transcription factors implicated in polarization of M2 and/or M2-like wound healing macrophages [26] were higher in CD11b$^+$ cells from LPLs of WT mice as compared to KO mice. Accordingly, increased expression of genes coding for anti-inflammatory functions, such as IL-1Ra, IL-10, TGFβ, arginase 1, COX2, and IDO, and those for wound healing functions, such as VEGF, FIZZ1, and MerTK, were upregulated in CD11b$^+$ of WT mice (Figure 4B) [20]. Somewhat surprisingly, expression levels of mRNA for transcription factors linked to proinflammatory M1 macrophages, such as AKT2, IRF3, and IRF5 were also higher in CD11b$^+$ macrophages from WT mice (Figure 4A). Inversely, the expression level of Ym-1, one of a maker for M2 macrophages with anti-inflammatory function, was lower in CD11b$^+$ macrophages from WT mice (Figure 4B).

Extrinsic IL-17 induces differentiation of blood monocytes into CD11b$^+$Ly6C$^+$MHC Class II$^+$ macrophages in the inflamed colon

Based on the finding that the expression level of CCL2 mRNA was increased in the inflamed colons and CCR2 was expressed on Ly6C$^+$MHC Class II$^+$ cells within CD11b$^+$ cells (Figure 2 and 3C), we next sought to determine whether CCR2$^+$Ly6C$^+$ blood monocytes are recruited predominantly to the inflamed colon and differentiate in situ under the influence of IL-17 into CD11b$^+$Ly6C$^+$MHC Class II$^+$ macrophages. To this end, monocytes were adoptively transferred into IL-17 sufficient or deficient mice, which received DSS treatment thereafter. On day 10, LPLs were harvested from these mice, among which donor cells were identified based on congenic markers and evaluated for their cell surface phenotype. As a representative result shown in Figure 5, most of donor monocytes, regardless of whether they were from WT or IL-17KO mice, gained MHC Class II expression and maintained Ly6C expression in WT host, whereas only a fraction of them gained MHC Class II in IL-17KO host. These results suggest that IL-17 is involved in the phenotypic and possibly functional maturation of monocytes by extrinsic mechanism.

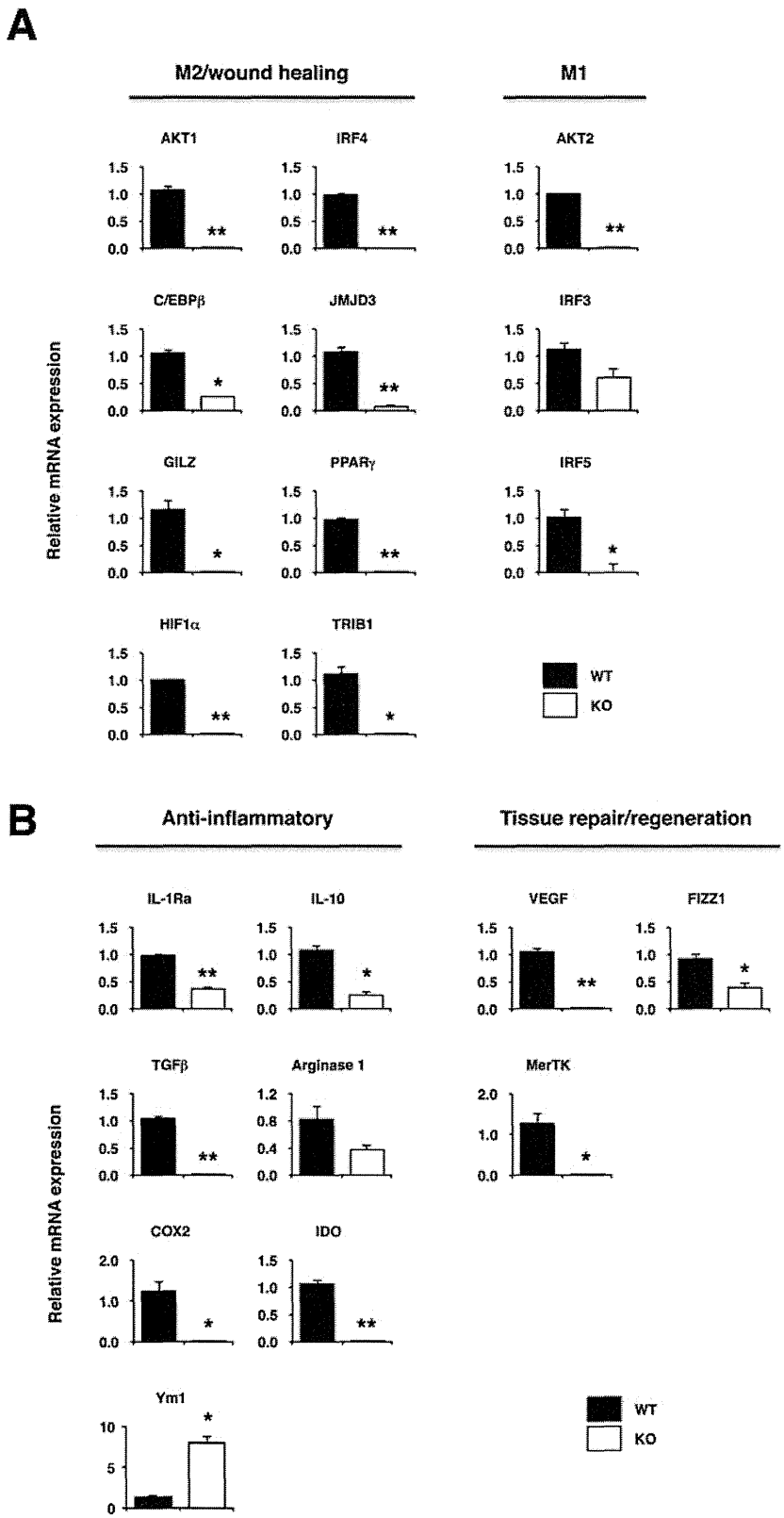

Figure 4. CD11b$^+$ cells from inflamed colonic LPLs of KO mice express significantly lower levels of genes implicated in M2/wound healing macrophages. IL-17KO mice and WT controls (n = 3) were treated with DSS as described in the legend for Figure 1. Then, LPLs isolated from these mice were further purified into CD11b$^+$ cell on FACS Aria, from which cDNA were prepared and subjected to real-time PCR analysis.

Expression of target mRNA were normalized to the expression of β-actin mRNA for generation of ΔCt values, and relative mRNA expression was quantified with the ΔΔCt method. Data are expressed as mean ± SEM. *$p<0.05$; **$p<0.01$.
doi:10.1371/journal.pone.0108494.g004

Depletion of CD11b$^+$Ly6C$^+$MHC Class II$^+$ macrophages exacerbates colon inflammation induced by DSS

Having confirmed that IL-17KO mice suffering more severe colitis had impaired ability to generate Ly6C$^+$MHC Class II$^+$ cells expressing the highest M2 marker within CD11b$^+$ cell population and CD11b$^+$ cells of the inflamed colonic LPLs from WT mice abundant in Ly6C$^+$MHC Class II$^+$ cells expressed increased level of most genes implicated in M2/wound healing macrophages (Figure 3 and 4), we next sought to determine whether CD11b$^+$Ly6C$^+$MHC Class II$^+$ cells are responsible for reduced colonic inflammation seen in WT mice. Liposome uptake by macrophages represents a genuine phagocytosis event [27], which has been widely used to target macrophage in vivo. Taking advantage of the fact that M2 macrophages have a high phagocytic activity [28] and intrarectal administration of clodronate-liposome, we could preferentially decrease Ly6C$^+$MHC Class II$^+$ over other subpopulations in LPLs, but not systemically, of DSS treated WT mice (Figure 6A and Figure S3). This treatment reduced colonic CD11b$^+$ cells by 35.6% (27.5±0.9% → 17.7±0.8%, $p<0.01$) and Ly6C$^+$MHC Class II$^+$ cells within CD11b$^+$ population by 35.4% (33.4±1.5% → 24.0±0.5%, $p<0.01$), resulting in an overall decrease in CD11b$^+$ Ly6C$^+$MHC Class II$^+$ macrophages by 53.9% (9.1±0.2% → 4.2±0.1%, $p<0.01$) in five independent experiments. On the other hand, mononuclear phagocyte populations as defined by CD11b, Ly6C and MHC Class II were marginally, if at all, affected in PBMC, spleen and bone marrow by this treatment (Figure S3). As expected, WT mice treated with clodronate-liposome exhibited a greater degree of body weight loss as compared to the mice treated with control-liposome (Figure 6B). Taken as a whole, these results indicate that CD11b$^+$Ly6C$^+$MHC Class II$^+$ macrophages differentiated from blood monocytes in the presence of IL-17 play a regulatory role in colonic inflammation.

Discussion

IL-17 has a critical function in the host defense response against various pathogens, but also has become notorious for its role in the pathogenesis of many inflammatory and autoimmune disorders, which makes this cytokine categorized as a proinflammatory cytokine [3]. This prevailing view was also adopted in IBD where IL-17 and IL-17 producing cells were found abundantly in the affected tissue [4]. Indeed, numerous studies have demonstrated pro-colitogenic role of IL-17 in animal models of IBD [8–10,12]. However, challenging this view, other studies in animal models [11,13,14] and recent human clinical trials [29,30] have emerged to suggest that IL-17 plays a protective role. To reassess the role of IL-17 in IBD pathogenesis and underlying mechanisms involved, we adopted a well-know DSS-induced colitis model, namely WT or IL-17KO mice were given DSS in drinking water. Upon evaluation of ensuing colitis, we found that IL-17KO mice were much more susceptible than WT mice. In addition, expression

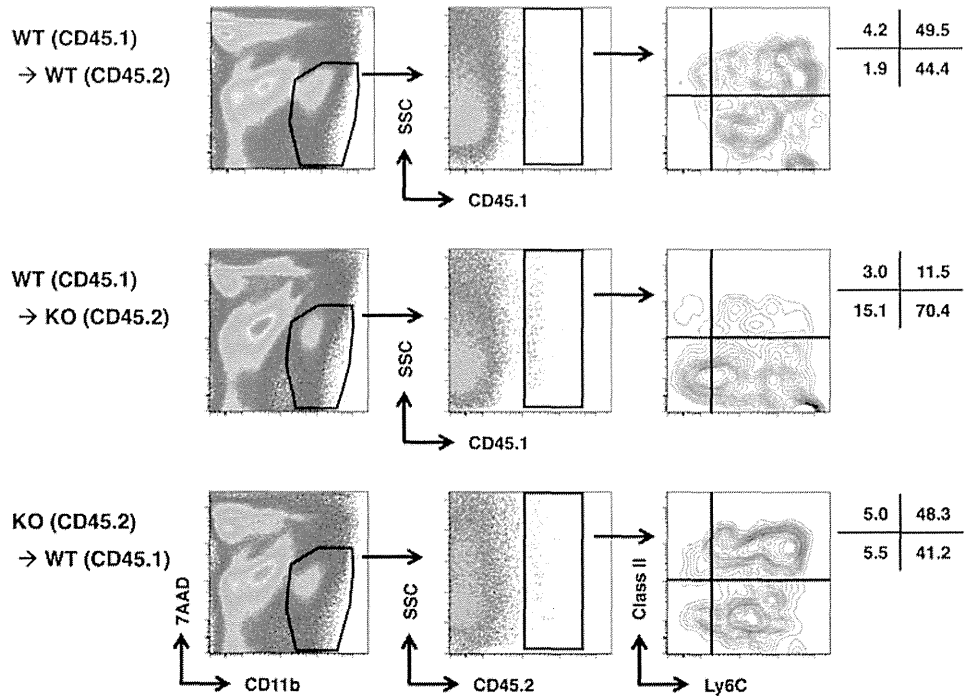

Figure 5. Blood monocytes are recruited into inflamed colons and differentiate into CD11b$^+$Ly6C$^+$MHC Class II$^+$ macrophages in the presence of IL-17. Monocytes were purified from bone marrow of WT (CD45.1), WT (CD45.2) or IL-17KO (CD45.2), and adaptively transferred into WT (45.2), IL-17KO (CD45.2) or WT (CD45.1) mice (n = 3), respectively, followed by the treatment with DSS. On day 10, colonic LPLs were isolated from pooled colon, stained with anti-CD11b, anti-Ly6C, and anti-MHC Class II together with corresponding anti-CD45 congenic antibody, and subjected to flow cytometry analysis. A representative result from three independent experiments is shown.
doi:10.1371/journal.pone.0108494.g005

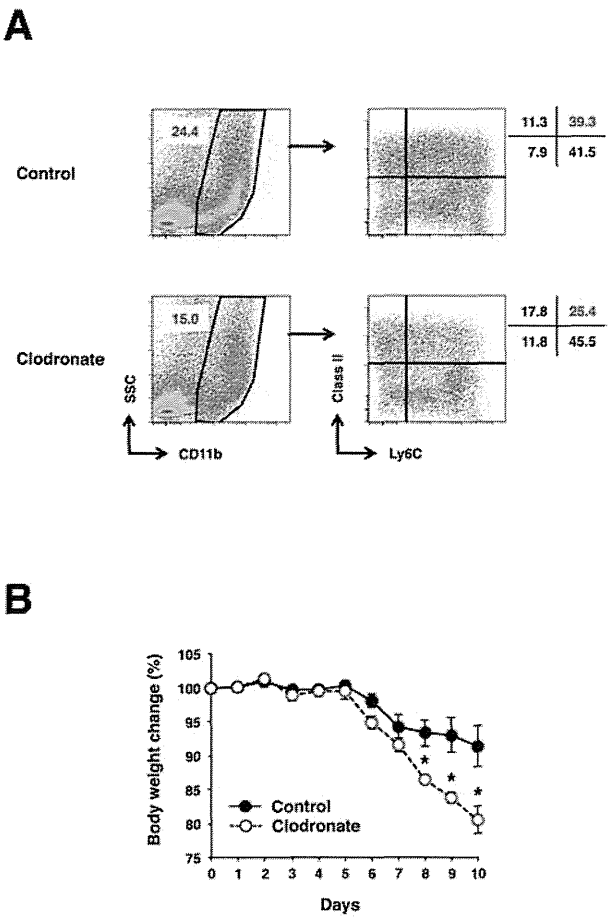

Figure 6. Depletion of CD11b$^+$Ly6C$^+$MHC Class II$^+$ macrophages accelerates colon inflammation in WT mice induced by DSS treatment. WT mice were given 1.5% DSS in drinking water for 7 days followed by consumption of water alone for another 3 days, during which the mice were treated with clodronate-liposome or control liposome intrarectally on days −1, 1, 3, and 5 as described in Materials and Methods. (A) Representative FACS plots showing reduced CD11b$^+$Ly6C$^+$MHC Class II$^+$ macrophages in colon of clodronate-liposome treated mice. (B) Changes in body weight over time were expressed as a percentage of the original weight. Data represent as mean ± SEM. The experiments were repeated two times with at least three mice per group per experiment.
doi:10.1371/journal.pone.0108494.g006

levels of mRNA coding for most, but not all, of the molecules contributing to suppression/resolution of inflammation and tissue repair [20,31] were significantly reduced in the inflamed colons of IL-17KO mice. Among those, genes expressed by M2/wound healing macrophages were downregulated in IL-17KO mice with notable consistency.

A characteristic of an inflammatory landscape in the colon of patients with IBD is an increased number of macrophages derived from blood monocytes [1,2]. As compared to a healthy colon, these macrophages produce an increased amount of inflammatory cytokines and express cell surface molecules involved in the activation of their own and T cells [1,2]. In a mouse model of colitis, these macrophages are CD11b$^+$F4/80$^+$MHC Class II$^+$CX3CR1^{int} driving inflammation through various effector mechanisms [25,32]. Hence, aberrant activation and functions of intestinal macrophages have been proposed to contribute to the IBD pathogenesis. However, recent studies also indicate that macrophages are functionally highly promiscuous, some of which also produce factors that dampen inflammatory responses while facilitating tissue repair [20,23,33]. Indeed, anti-TNF therapy for patients with IBD induces macrophages with regulatory functions, which promote wound healing [34]. In an animal model of colitis, macrophages have also been shown to exert disease ameliorating effects. These macrophages include CD11b$^+$F4/80$^+$MHC Class II$^+$ cells coexpressing CD11c and/or also CX3CR1 [35,36]. It has also been shown that they are recent emigrant from blood monocytes [37]. Recent study also points that CD64 as a specific macrophage marker that can discriminate dendritic cells from macrophages in the murine intestine under both steady-state and inflammatory conditions [24]. In our present study, we found a significant decrease in the frequency of CD11b$^+$Ly6C$^+$MHC Class II$^+$CD64$^+$ macrophages, which were derived, at least in part, from blood monocytes, in the inflamed colon of IL-17KO mice as compared to WT mice. Although statistically non-significant due to the variation in number of cells recovered from LPLs in each experiment, the absolute numbers of CD11b$^+$Ly6C$^+$MHC Class II$^+$ macrophages were almost consistently reduced in IL-17KO mice. Furthermore, depletion of this population by topical administration of clodronate-liposome resulted in the exacerbation of DSS-induced colitis in WT mice, clearly indicating that these macrophages ameliorate, rather than exacerbate, colitis. In support of this notion, recent studies have shown that CD11b$^+$Ly6C$^+$MHC Class II$^+$ macrophages in inflamed intestine produce both inflammatory and anti-inflammatory molecules to control invading pathogen while limiting collateral tissue damage [38,39]. Commercially available Abs do not allow to detect CX3CR1 by flow cytometry or immunohistochemistry, we were unable to determine whether CD11b$^+$Ly6C$^+$MHC Class II$^+$ macrophages express CX3CR1 and belong to the same or overlapping population mentioned above, an important issue which needs to be further investigated.

CD11b$^+$ cells isolated from the inflamed colons of WT mice enriched in CD11b$^+$Ly6C$^+$MHC Class II$^+$ macrophages expressed higher levels of mRNA encoding anti-inflammatory and tissue repair functions as compared to CD11b$^+$ cells from IL-17KO mice. A discrepancy remains, however, in that CD11b$^+$ cells from the inflamed colons of IL-17KO mice expressed higher levels of Ym1 mRNA, which is a marker for M2 macrophages [40]. Resent study indicates that GM-CSF is critical in the expression of Ym1 [41]. Therefore, the higher levels of GM-CSF in the inflamed colons of IL-17KO mice as compared to WT mice (data not shown) may explain this seemingly paradoxical observation. Taken as a whole, it is possible that through the production of factors with anti-inflammatory/tissue repair functions, CD11b$^+$Ly6C$^+$MHC Class II$^+$ macrophages suppress inflammation while quickly repairing colon tissue before serious damage to the tissue occurs, resulting in less severe colitis seen in WT mice. Recent studies also suggest that a subset of macrophages in the colon play a crucial role in the maintenance and/or promotion of differentiation of functional Foxp3$^+$ regulatory T cells. Together with our present results that inflamed colon of IL-17KO mice contained reduced levels of Foxp3$^+$ T cells, it is also possible that CD11b$^+$Ly6C$^+$MHC Class II$^+$ macrophages ameliorate colitis through enhancement of Foxp3$^+$ regulatory T cell function [23]. In support of this notion, we observed that the depletion of CD11b$^+$Ly6C$^+$MHC Class II$^+$ macrophages in colon of WT mice by clodronate-liposome was associated with the reduction in Foxp3$^+$CD4$^+$T cells by 36% (30.3±0.63% → 19.2±0.62%, $p < 0.01$, $n = 4$).

Perhaps more importantly, our study revealed that monocytes differentiate to express molecules and genes implicated in M2/wound healing macrophages under the influence of IL-17 in the inflamed colon. In support of this notion, recent studies show that IL-17 stimulates differentiation of M2/anti-inflammatory macrophages [42,43]. However, in the present study we showed that along with elevated expression of mRNA for M2 associated transcription factors and anti-inflammatory/tissue regenerative factors, $CD11b^+$ myeloid cells in the inflamed colons of WT mice also expressed higher levels of mRNA for M1 associated transcription factors. Thus, macrophages differentiated under the influence of IL-17 did not fit comfortably with the M1/M2-paradigm of differentiated macrophages. We speculate that macrophages may acquire the unique M2 dominant properties adapted to the inflamed colon microenvironment under the influence of a unique cytokine milieu involving IL-17.

In summary, our study shows, for the first time, that $CD11b^+Ly6C^+$MHC Class II^+ macrophages differentiated in the inflamed colon under the influence of IL-17 represent M2-like/wound healing macrophages which may have regulatory functions. Whether the induction of this population by IL-17 solely explains all of the protective function of IL-17 in colitis remains arguable, since we also observed that inflamed colonic tissue of IL-17KO mice expressed reduced levels of claudin-1/2, β-difensin-1/2, and mucin-2, all of which have been shown to be regulated by IL-17 signaling. However, our data demonstrate a previously unappreciated mechanism by which IL-17 exerts protective functions in colitis and targeting IL-17/M2-like macrophage axis may represent an important future therapeutic approach in the treatment of mucosal inflammatory diseases such as IBD.

Supporting Information

Figure S1 Flow cytometric analysis of LPL from WT and IL-17KO mice. IL-17KO mice and WT controls were given 1.5% DSS in drinking water for 7 days followed by consumption of water alone for another 3 days. LPLs were purified from pooled (n = 2–3) distal colon sections of untreated and DSS-treated mice and subjected to flow cytometry analysis after staining with mAbs specific for indicated cell surface and intracellular molecules. Plots were shown after electric gating for $7AAD^-$ and $CD45^+$ cells. Number denotes frequency of gated cells. Representative results of at least two independent experiments are shown.
(TIF)

Figure S2 Flow cytometry analysis of $CD11b^+$ cells before and after cell sorting. IL-17KO mice and WT controls were given 1.5% DSS in drinking water for 7 days followed by consumption of water alone for another 3 days. LPLs were purified from pooled (n = 10) distal colon sections of untreated and DSS-treated mice followed by cell sorting by FACS. Representative results out of two independent experiments are shown.
(TIF)

Figure S3 Representative flow cytometry plots on $CD11b^+Ly6C^+$MHC Class II^+ macrophage population in organs other than colon of WT mice treated with clodronate-liposome. WT mice were given 1.5% DSS in drinking water for 7 days followed by consumption of water alone for another 3 days, during which the mice were treated with clodronate-liposome or control liposome intrarectally on days −1, 1, 3, and 5 and their body weight changes were monitored. The experiments were repeated two times with at least tree mice per group per experiment.
(TIF)

Table S1 Primer sequences used for realtime RT-PCR.
(DOCX)

Acknowledgments

The authors thank Mrs. Kazuko Shirakura for her skilled technical assistance for cell sorting.

Author Contributions

Conceived and designed the experiments: KN TK. Performed the experiments: KN NS TK NM. Analyzed the data: KN TK. Contributed reagents/materials/analysis tools: DM IT MM KT YT MT HS NK. Contributed to the writing of the manuscript: KN TK.

References

1. Kaser A, Zeissig S, Blumberg RS (2010) Inflammatory bowel disease. Annu Rev Immunol 28: 573–621.
2. Strober W, Fuss IJ, Mannon P (2007) The fundamental basis of inflammatory bowel disease. J Clin Invest 117: 514–521.
3. Iwakura Y, Ishigame H, Saijo S, Nakae S (2011) Functional specialization of interleukin-17 family members. Immunity 34: 149–162.
4. Fujino S, Andoh A, Bamba S, Ogawa A, Hata K, et al. (2003) Increased expression of interleukin 17 in inflammatory bowel disease. Gut 52: 65–70.
5. Hue S, Ahern PP, Buonocore S, Kullberg MC, Cua DJ, et al. (2006) Interleukin-23 drives innate and T cell-mediated intestinal inflammation. J Exp Med 203: 2473–2483.
6. Tang C, Iwakura Y (2012) IL-23 in colitis: targeting the progenitors. Immunity 37: 957–959.
7. Hundorfean G, Neurath MF, Mudter J (2012) Functional relevance of T helper 17 (Th17) cells and the IL-17 cytokine family in inflammatory bowel disease. Inflamm Bowel Dis 18: 180–186.
8. Zhang Z, Zheng M, Bindas J, Schwarzenberger P, Kolls JK (2006) Critical role of IL-17 receptor signaling in acute TNBS-induced colitis. Inflamm Bowel Dis 12: 382–388.
9. Buonocore S, Ahern PP, Uhlig HH, Ivanov II, Littman DR, et al. (2010) Innate lymphoid cells drive interleukin-23-dependent innate intestinal pathology. Nature 464: 1371–1375.
10. Chaudhry A, Rudra D, Treuting P, Samstein RM, Liang Y, et al. (2009) $CD4^+$ regulatory T cells control TH17 responses in a Stat3-dependent manner. Science 326: 986–991.
11. O'Connor W, Kamanaka M, Booth CJ, Town T, Nakae S, et al. (2009) A protective function for interleukin 17A in T cell-mediated intestinal inflammation. Nat Immunol 10: 603–609.
12. Ito R, Kita M, Shin-Ya M, Kishida T, Urano A, et al. (2008) Involvement of IL-17A in the pathogenesis of DSS-induced colitis in mice. Biochem Biophys Res Commun 377: 12–16.
13. Ogawa A, Andoh A, Araki Y, Bamba T, Fujiyama Y (2004) Neutralization of interleukin-17 aggravates dextran sulfate sodium-induced colitis in mice. Clin Immunol 110: 55–62.
14. Yang XO, Chang SH, Park H, Nurieva RI, Shah B, et al. (2008) Regulation of inflammatory responses by IL-17F. J Exp Med 205: 1063–1075.
15. Nakae S, Komiyama Y, Nambu A, Sudo K, Iwase M, et al. (2002) Antigen-specific T cell sensitization is impaired in IL-17-deficient mice, causing suppression of allergic cellular and humoral responses. Immunity 17: 375–387.
16. Schepp-Berglind J, Atkinson C, Elvington M, Qiao F, Mannon P, et al. (2012) Complement-dependent injury and protection in a murine model of acute dextran sulfate sodium-induced colitis. J Immunol 188: 6309–6318.
17. Varol C, Vallon-Eberhard A, Elinav E, Aychek T, Shapira Y, et al. (2009) Intestinal lamina propria dendritic cell subsets have different origin and functions. Immunity 31: 502–512.
18. Wang L, Toda M, Saito K, Hori T, Horii T, et al. (2008) Post-immune UV irradiation induces Tr1-like regulatory T cells that suppress humoral immune responses. Int Immunol 20: 57–70.
19. Torii M, Wang L, Ma N, Saito K, Hori T, et al. (2010) Thioredoxin suppresses airway inflammation independently of systemic Th1/Th2 immune modulation. Eur J Immunol 40: 787–796.
20. Gordon S, Martinez FO (2010) Alternative activation of macrophages: mechanism and functions. Immunity 32: 593–604.
21. Monteleone I, Rizzo A, Sarra M, Sica G, Sileri P, et al. (2011) Aryl Hydrocarbon Receptor-Induced Signals Up-regulate IL-22 Production and

Inhibit Inflammation in the Gastrointestinal Tract. Gastroenterology 141: 237–248. e231.
22. Hansell CAH, Hurson CE, Nibbs RJB (2011) DARC and D6: silent partners in chemokine regulation? Immunol Cell Biol 89: 197–206.
23. Zigmond E, Jung S (2013) Intestinal macrophages: well educated exceptions from the rule. Trends Immunol 34: 162–168.
24. Tamoutounour S, Henri S, Lelouard H, de Bovis B, de Haar C, et al. (2012) CD64 distinguishes macrophages from dendritic cells in the gut and reveals the Th1-inducing role of mesenteric lymph node macrophages during colitis. Eur J Immunol 42: 3150–3166.
25. Rivollier A, He J, Kole A, Valatas V, Kelsall BL (2012) Inflammation switches the differentiation program of Ly6Chi monocytes from antiinflammatory macrophages to inflammatory dendritic cells in the colon. J Exp Med 209: 139–155.
26. Lawrence T, Natoli G (2011) Transcriptional regulation of macrophage polarization: enabling diversity with identity. Nat Rev Immunol 11: 750–761.
27. Perry DG, Martin WJ (1995) Fluorescent liposomes as quantitative markers of phagocytosis by alveolar macrophages. J Immunol Methods 181: 269–285.
28. Leidi M, Gotti E, Bologna L, Miranda E, Rimoldi M, et al. (2009) M2 macrophages phagocytose rituximab-opsonized leukemic targets more efficiently than m1 cells in vitro. J Immunol 182: 4415–4422.
29. Targan SR, Feagan BG, Vermeire S, Panaccione R, Melmed GY, et al. (2012) Mo2083 A Randomized, Double-Blind, Placebo-Controlled Study to Evaluate the Safety, Tolerability, and Efficacy of AMG 827 in Subjects With Moderate to Severe Crohn's Disease. Gastroenterology 143: e26.
30. Hueber W, Sands BE, Lewitzky S, Vandemeulebroecke M, Reinisch W, et al. (2012) Secukinumab, a human anti-IL-17A monoclonal antibody, for moderate to severe Crohn's disease: unexpected results of a randomised, double-blind placebo-controlled trial. Gut.
31. Zizzo G, Hilliard BA, Monestier M, Cohen PL (2012) Efficient clearance of early apoptotic cells by human macrophages requires M2c polarization and MerTK induction. J Immunol 189: 3508–3520.
32. Kostadinova FI, Baba T, Ishida Y, Kondo T, Popivanova BK, et al. (2010) Crucial involvement of the CX3CR1-CX3CL1 axis in dextran sulfate sodium-mediated acute colitis in mice. J Leukocyte Biol 88: 133–143.
33. Mantovani A, Biswas SK, Galdiero MR, Sica A, Locati M (2013) Macrophage plasticity and polarization in tissue repair and remodelling. J Pathol 229: 176–185.
34. Vos ACW, Wildenberg ME, Duijvestein M, Verhaar AP, Van Den Brink GR, et al. (2011) Anti-tumor necrosis factor-α antibodies induce regulatory macrophages in an Fc region-dependent manner. Gastroenterology 140: 221–230.
35. Kayama H, Ueda Y, Sawa Y, Jeon SG, Ma JS, et al. (2012) Intestinal CX3C chemokine receptor 1(high) (CX3CR1(high)) myeloid cells prevent T-cell-dependent colitis. Proc Natl Acad Sci U S A 109: 5010–5015.
36. Qualls JE, Kaplan AM, Van Rooijen N, Cohen DA (2006) Suppression of experimental colitis by intestinal mononuclear phagocytes. J Leukocyte Biol 80: 802–815.
37. Medina-Contreras O, Geem D, Laur O, Williams IR, Lira SA, et al. (2011) CX3CR1 regulates intestinal macrophage homeostasis, bacterial translocation, and colitogenic Th17 responses in mice. J Clin Invest 121: 4787–4795.
38. Bain CC, Scott CL, Uronen-Hansson H, Gudjonsson S, Jansson O, et al. (2013) Resident and pro-inflammatory macrophages in the colon represent alternative context-dependent fates of the same Ly6Chi monocyte precursors. Mucosal Immunol 6: 498–510.
39. Grainger JR, Wohlfert EA, Fuss IJ, Bouladoux N, Askenase MH, et al. (2013) Inflammatory monocytes regulate pathologic responses to commensals during acute gastrointestinal infection. Nat Med 19: 713–721.
40. Nair MG, Cochrane DW, Allen JE (2003) Macrophages in chronic type 2 inflammation have a novel phenotype characterized by the abundant expression of Ym1 and Fizz1 that can be partly replicated in vitro. Immunol Lett 85: 173–180.
41. Chen GH, Olszewski MA, McDonald RA, Wells JC, Paine R 3rd, et al. (2007) Role of granulocyte macrophage colony-stimulating factor in host defense against pulmonary Cryptococcus neoformans infection during murine allergic bronchopulmonary mycosis. Am J Pathol 170: 1028–1040.
42. Liu L, Ge D, Ma L, Mei J, Liu S, et al. (2012) Interleukin-17 and prostaglandin E2 are involved in formation of an M2 macrophage-dominant microenvironment in lung cancer. J Thorac Oncol 7: 1091–1100.
43. Zizzo G, Cohen PL (2013) IL-17 stimulates differentiation of human anti-inflammatory macrophages and phagocytosis of apoptotic neutrophils in response to IL-10 and glucocorticoids. J Immunol 190: 5237–5246.

OPEN ACCESS Freely available online

PLOS ONE

Systemic CD8$^+$ T Cell-Mediated Tumoricidal Effects by Intratumoral Treatment of Oncolytic Herpes Simplex Virus with the Agonistic Monoclonal Antibody for Murine Glucocorticoid-Induced Tumor Necrosis Factor Receptor

Mikiya Ishihara[1], Naohiro Seo[1]*, Jun Mitsui[2], Daisuke Muraoka[1], Maki Tanaka[3], Junichi Mineno[3], Hiroaki Ikeda[1], Hiroshi Shiku[1]*

1 Department of Immuno-Gene Therapy, Mie University Graduate School of Medicine, Mie, Japan, **2** Department of Gastroenterological Surgery II, Hokkaido University Graduate School of Medicine, Hokkaido, Japan, **3** Gene Medicine Business Unit, Takara Bio Inc., Shiga, Japan

Abstract

Oncolytic virotherapy combined with immunomodulators is a novel noninvasive strategy for cancer treatment. In this study, we examined the tumoricidal effects of oncolytic HF10, a naturally occurring mutant of herpes simplex virus type-1, combined with an agonistic DTA-1 monoclonal antibody specific for the glucocorticoid-induced tumor necrosis factor receptor. Two murine tumor models were used to evaluate the therapeutic efficacies of HF10 virotherapy combined with DTA-1. The kinetics and immunological mechanisms of DTA-1 in HF10 infection were examined using flow cytometry and immunohistochemistry. Intratumoral administration of HF10 in combination with DTA-1 at a low dose resulted in a more vigorous attenuation of growth of the untreated contralateral as well as the treated tumors than treatment with either HF10 or DTA-1 alone. An accumulation of CD8$^+$ T cells, including tumor- and herpes simplex virus type-1-specific populations, and a decrease in the number of CD4$^+$ Foxp3$^+$ T regulatory cells were seen in both HF10- and DTA-1-treated tumors. Studies using Fc-digested DTA-1 and Fcγ receptor knockout mice demonstrated the direct participation of DTA-1 in regulatory T cell depletion by antibody-dependent cellular cytotoxicity primarily via macrophages. These results indicated the potential therapeutic efficacy of a glucocorticoid-induced tumor necrosis factor receptor-specific monoclonal antibody in oncolytic virotherapy at local tumor sites.

Citation: Ishihara M, Seo N, Mitsui J, Muraoka D, Tanaka M, et al. (2014) Systemic CD8$^+$ T Cell-Mediated Tumoricidal Effects by Intratumoral Treatment of Oncolytic Herpes Simplex Virus with the Agonistic Monoclonal Antibody for Murine Glucocorticoid-Induced Tumor Necrosis Factor Receptor. PLoS ONE 9(8): e104669. doi:10.1371/journal.pone.0104669

Editor: Claude Krummenacher, University of Pennsylvania School of Veterinary Medicine, United States of America

Received April 30, 2014; **Accepted** July 11, 2014; **Published** August 8, 2014

Data Availability: The authors confirm that all data underlying the findings are fully available without restriction. All relevant data are within the paper and its Supporting Information files.

Funding: This work was supported by grants from Ministry of Education, Culture, Sports, Science and Technology of Japan (24390300 and 24800033). The funders had no role in study design, data collection and analysis, decision to publish, or preparation of the manuscript.

Competing Interests: The authors have declared that no competing interests exist. Specifically, the following co-authors: M. Tanaka and J. Mineno confirm that, in spite of them being employed by commercial companies Takara Bio Inc., this does not alter the authors' adherence to all the PLOS ONE policies on sharing data and materials and that they are entitled and allowed to publish the results reported in this manuscript. H. Shiku is a PLOS ONE Editorial Board member. This does not alter the authors' adherence to PLOS ONE Editorial policies and criteria.

* Email: seo-naohiro@clin.medic.mie-u.ac.jp (NS); shiku@clin.medic.mie-u.ac.jp (HS)

Introduction

Oncolytic virotherapy has existed for over 100 years and is a promising method for the treatment of cancer patients because of the strong cytolytic response of virus-infected tumor cells; however, complications may result from the use of oncolytic viruses including toxicity against normal cells [1–3]. Thus, artificially modified oncolytic viruses have been engineered to achieve low toxicity against normal tissues together with sufficient antitumor activity. Oncolytic viruses that have been modified to express human cytokines, such as granulocyte macrophage colony-stimulating factor (GM-CSF) have the potential for future therapeutic use in the treatment of solid tumors. JX-594 is a GM-CSF-armed oncolytic poxvirus that has shown promising outcomes when administered by either intratumoral (i.t.) injection or intravenous (i.v.) infusion [4–8]. OncoVEX$^{GM\text{-}CSF}$ is an oncolytic virus based on the JS-1 strain of herpes simplex virus type-1 (HSV-1) that has been engineered to express human GM-CSF [9–12]. The results of a phase III trial demonstrate that melanoma patients treated with this virus show statistically significant improvement with durable responses [12].

HSV infection in wide ranges of cell populations results in degenerative change and death [13]. HF10 is a spontaneous mutant of HSV-1 strain HF [14] that lacks neuroinvasiveness and is at least 10,000-fold less virulent than wild-type HSV-1 in mice [15]. In several clinical studies of cancer patients, HF10 has been shown to have antitumor effects [16–19]. In murine studies, HF10 packaged with a GM-CSF-expressing amplicon has been reported to exhibit more tumoricidal activity than intact HF10 [20,21], supporting the hypothesis that HF10 exhibits maximal antitumor activity when used in combination with immunomodulators.

Glucocorticoid-induced tumor necrosis factor receptor (GITR) is a type I transmembrane protein of the tumor necrosis factor receptor family, and is involved in the regulation of T-cell receptor-mediated cell death [22]. GITR is similar to programmed cell death-1 (PD-1) and cytotoxic T-lymphocyte antigen 4 (CTLA-4), both of which have been applied clinically as immune modifiers in tumor therapy [23]. GITR has been reported to be expressed at high levels on $CD4^+$ $CD25^+$ regulatory T (Treg) cells and to abrogate Treg cell-mediated immune suppression via intercellular signaling [24,25]. GITR has also been known to be expressed on activated $CD8^+$ T cells and to act on the induction of tumor-specific $CD8^+$ T cells [26]. In addition, GITR signaling via specific ligands seems to drive $CD8^+$ T cell resistance to Treg cell-mediated inhibition [27]. Currently there is an ongoing clinical trial of a therapeutic anti-human GITR antibody [28]. Thus, GITR targeting is an attractive candidate method for use in HF10 virotherapy as it encourages tumoricidal cytotoxic T lymphocyte (CTL) activity and attenuates immune suppression.

In this study, we examined the anti-tumor effects of i.t. treatment of established murine tumors with HF10 in combination with the GITR-specific agonistic monoclonal antibody (mAb) DTA-1. Our results show that the combination therapy inhibited tumor growth at the contralateral as well as the injected tumor sites by promoting the accumulation of tumor-specific $CD8^+$ T cells followed by DTA-1-mediated depletion of $CD4^+$ $Foxp3^+$ Treg cells. Thus, DTA-1 is an extremely effective partner for HF10 in oncolytic virotherapy.

Materials and Methods

Mice

Female BALB/c mice aged 6–8 weeks were obtained from SLC Japan. BALB/c mice deficient in the γ subunit of the FcγRI, FcγRIII and FcεRI receptors (FcRγ KO mice) [29] were purchased from Taconic and bred at the Mie University Institute of Laboratory Animals. Experimental protocols were approved by the Animal Ethics Committee of Mie University, Tsu, Japan (Approval number: 23-8).

Cell lines

CT26 is a colon tumor cell line derived from BALB/c mice [30]. A CT26 cell line transfected with the gene encoding the human cancer/testis antigen NY-ESO-1 (CT26/NY-ESO-1) was established as described previously [31]. CMS5a is a 3-methyl cholanthrene-induced fibrosarcoma cell line derived from BALB/c mice [32]. A CMS5a cell line transfected with the gene encoding GITR was established by retrovirus-mediated gene transfer. The retrovirus containing the murine GITR gene was purchased from Takara Bio Inc.

CT26/NY-ESO-1 and CMS5a cells were inoculated subcutaneously (s.c.) into the hind flanks of mice (1×10^6 cells/mouse and 2×10^5 cells/mouse, respectively). HF10 or the vehicle was administered i.t. (1×10^7 PFU/mouse) at 7, 8, and 9 days after tumor inoculation. DTA-1 was administered i.t. (10 μg/mouse) at 9 days after tumor inoculation. For the combination therapy, 10 μg of DTA-1 were mixed with the HF10 virus and administered to the mice at 9 days after tumor inoculation.

Antibodies

Fluorescein isothiocyanate (FITC)-conjugated and/or phycoerythrin (PE)-conjugated anti-mouse CD4 (RM4-5; eBioscience, Inc), anti-mouse CD8α mAb (53-6.7; BD Bioscience), anti-mouse/rat Foxp3 mAb (FJK-16s; eBioscience, Inc), anti-mouse IFN-γ mAb (XMG1.2; eBioscience, Inc), anti-mouse F4/80 mAb (BM8; BioLegend), and anti-rat IgG2b monoclonal antibodies (mAbs) (MRG2b-85; BioLegend) as well as a FITC-conjugated rabbit anti-HSV-1 polyclonal antibody (Dako) were used in flow cytometric analysis and immunohistochemstry. An anti-mouse CD16/CD32 mAb (93; eBioscience, Inc) was used for Fc-blocking in all experiments. For *in vivo* administration, anti-mouse GITR mAb (DTA-1, rat IgG2b) and anti-mouse CD8α mAb were purified by protein G affinity column chromatography of ascites from BALB/c nude mice intraperitoneally inoculated with a 53-6.7 hybridoma. Purifed rat serum IgG (Sigma) was used as the control antibody for all experiments with DTA-1. The Fab portion of DTA-1 was prepared by using a Pierce Fab Preparation Kit (Thermo Fisher Scientific) according to the manufacturer's instructions.

Cell preparations

To collect tumor-infiltrating lymphocytes (TILs), a gentleMACS dissociator (Miltenyi Biotec K.K.) was used according to the manufacturer's instructions with some modifications. Briefly, a CT26/NY-ESO-1 tumor cut into small pieces was incubated in 4.5 mL of RPMI-1640 medium supplemented with 1 mg/mL collagenase IA (Sigma) for 40 min at 37°C and then dissociated into single cells using the gentleMACS dissociator. DNase I was not used. The obtained cells were passed through a cell strainer (70 μm) to remove tissue aggregates. After washing 3 times with PBS containing 0.1% BSA, the TILs were evaluated by flow cytometric analysis for intracellular IFN-γ as described below. When DTA-1-binding TIL populations were studied, collagenase I was not used so as to avoid the dissociation of DTA-1 bound to cells.

To investigate DTA-1-mediated generation of tumor-specific $CD8^+$ T cells, DTA-1 was injected i.t. into day 9 CT26/NY-ESO-1 tumors at three doses (0.5, 2, or 10 μg). Tumor-regressed mice were selected from each DTA-1-treated group at 2 weeks after DTA-1 treatment, and the splenocytes from each group were pooled and incubated in RPMI-1640 medium supplemented with 10% fetal calf serum (FCS) and 10 μg/mL of control peptide (9 m: QYIHSANVL) [32], CT26-specific AH-1 peptide (SPSYVYHQF) [33] or NY-ESO-1_{81-88} peptide (RGPESRLL) [34] (all from MBL) for 5 hrs. The obtained cells were analyzed by flow cytometry to determine levels of intracellular IFN-γ.

Splenocytes from CT26/NY-ESO-1-bearing mice obtained at 5 days after i.t. treatment with both HF10 (days 7, 8 and 9) and DTA-1 (day 9) were cultured with CT26-specific AH-1 peptide (10 μg/mL) or HF10-infected CMS5a tumor cells [precultured with HF10 (MOI 1) for 12 hrs and irradiated with 50 Gy] at a ratio of 5 splenocytes to 1 HF10-infected CMS5a cell for 5 hrs. The obtained cells were then evaluated for intracellular IFN-γ as described below.

Flow cytometric analysis of mAb-stained cells

To confirm GITR expression on CMS5a/GITR cells, CMS5a/GITR cells were incubated with DTA-1 ($<2\times10^6$ cells/μg in PBS supplemented with 0.2% BSA) for 15 min at 4°C. After washing 3 times with PBS containing 0.1% BSA, the cells were further treated with FITC-conjugated anti-rat IgG (H + L) Ab (Caltag Lab.) ($<2\times10^6$ cells/μg) for 15 min at 4°C. For staining of intracellular IFN-γ in cultured splenic $CD8^+$ T cells, GolgiPlug (BD Bioscience) protein transport inhibitor was added for the last 4 hrs of the incubation. The obtained cells were permeabilized using a Cytofix/Cytoperm Kit (BD Bioscience) and stained with a CD8α-specific mAb for 15 min at 4°C and followed by an IFN-γ-specific mAb for 15 min at 4°C ($<2\times10^6$ cells/μg). For Foxp3-CD4 double labeling of TILs, TILs were first stained with a CD4-

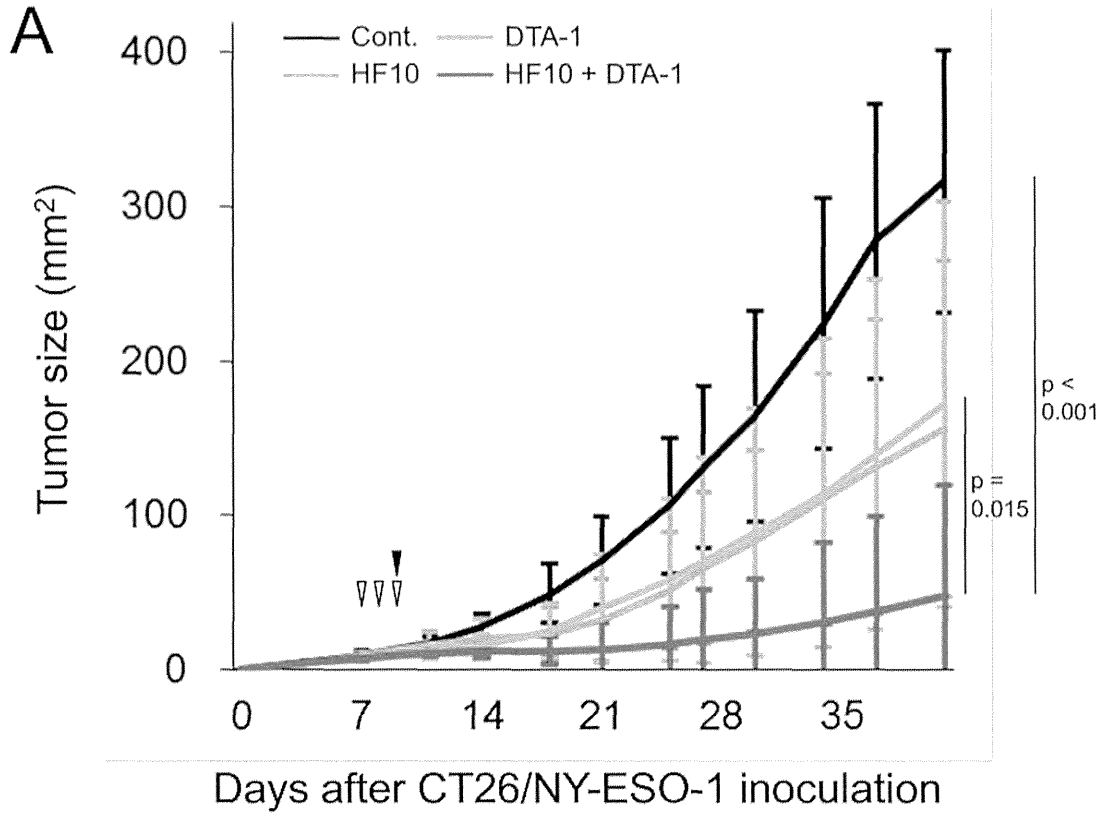
A
Cont.
DTA-1
HF10
HF10 + DTA-1
Tumor size (mm2)
400
300
200
100
0
0
7
14
21
28
35
p < 0.001
p = 0.015
Days after CT26/NY-ESO-1 inoculation

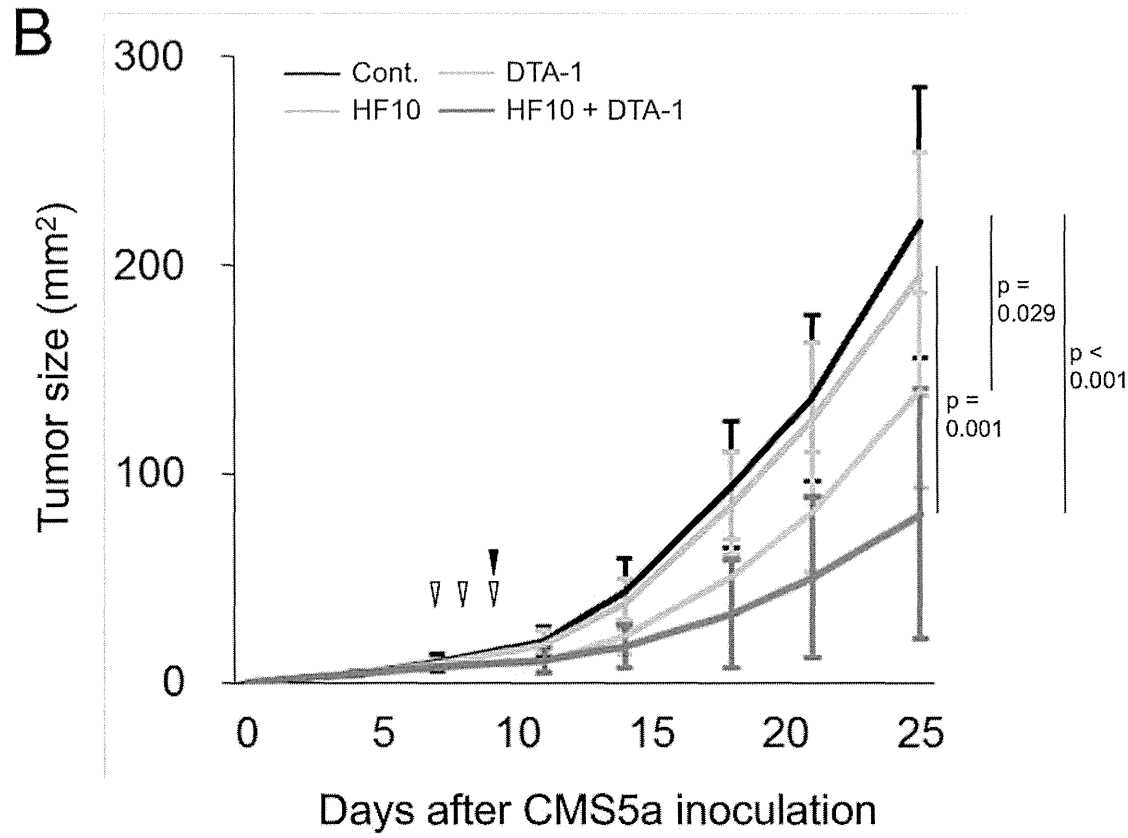
B
Cont.
DTA-1
HF10
HF10 + DTA-1
Tumor size (mm2)
300
200
100
0
0
5
10
15
20
25
p = 0.029
p < 0.001
p = 0.001
Days after CMS5a inoculation

Figure 1. Tumor growth following intratumoral administration of HF10 with/without DTA-1. Growth (mm^2) of subcutaneously inoculated CT26/NY-ESO-1 (A) or CMS5a cells (B) following i.t. treatment with HF10 (open triangles) and/or DTA-1 (closed triangles) on indicated days. Purified rat IgG was used as a control for DTA-1. Data shown in Fig. 1 are representative of four independent experiments. By the Kruskal-Wallis ANOVA test, the CT26/NY-ESO-1 growth inhibition by combined treatment with HF10 and DTA-1 was significantly different from the HF10-treated or untreated control at day 42. CMS5a growth inhibition by the HF10 and DTA-1 combination was significantly different from the DTA-1-treated or untreated control at day 25. CMS5a growth inhibition was also significantly different in the HF10-treated group compared with the untreated control.
doi:10.1371/journal.pone.0104669.g001

specific mAb [15 min, 4°C ($<2\times10^6$ cells/μg)], then fixed and permeabilized using a Foxp3 staining kit (eBioscience, Inc.), and then treated with a Foxp3-specific mAb [30 min, 4°C ($<1\times10^6$ cells/μg)]. The labeled cells were then analyzed by flow cytometry (FACSCanto II: BD Bioscience) with FlowJo software (Tomy Digital Biology).

Immunohistochemistry

Frozen CT26/NY-ESO-1 tumor specimens embedded in O.C.T compound (Sakura Finetechnical) were sectioned at a thickness of 3 μm, air dried for 2 hrs, fixed with cold acetone for 15 min, and then processed for immunohistochemistry. After washing 3 times with PBS, the slides were incubated at 4°C in blocking solution [PBS supplemented with 1% BSA, 5% Blocking One Histo (Nacalai Tesque, Inc.)] and 0.2 μg/mL anti-mouse CD16/CD32 mAb for 30 min. The tumor sections on the slides were then dual-labeled with PE-conjugated mAb and FITC-conjugated mAb diluted with PBS supplemented with 1% BSA and 5% Blocking One Histo for 1 hr at room temperature (r.t.) in a humidified chamber. After washing 3 times with PBS supplemented with 0.02% Tween-20, the slides were mounted in ProLong Gold antifade reagent with DAPI (Invitrogen, Life Technologies, Inc.), and evaluated by fluorescence microscopy (BX53F; Olympus Co. Ltd.; Tokyo, Japan). The photographs from PE-, FITC-, and DAPI-stained tissue sections were merged and background fluorescence was deleted using Photoshop elements software (Adobe Systems Software Ltd.).

For hematoxylin and eosin (HE) staining, slides with acetone-fixed tissue sections were washed 3 times with PBS and incubated at r.t. in hematoxylin solution (New Hematoxylin Sol.: Muto Pure Chemicals Co., Ltd.) for 5 min. After washing with tap water, the cytoplasm was stained with eosin (r.t. for 2 min.; Pure Eosin Sol.: Muto Pure Chemicals). Samples were then dehydrated 3 times with xylene, and the slides were mounted with Malinol (Muto Pure Chemicals) and evaluated by microscopy.

Antibody-dependent cellular cytotoxicity (ADCC) assay

RAW264.7 cells were activated with 20 ng/mL murine IFN-γ for 24 hrs in 24-well plates, after which the cells were gently washed with RPMI-1640 and the dish-adherent RAW264.7 cells were used as effectors in the ADCC assay. CMS5a or CMS5a/GITR cells were labeled with 2.5 μM carboxyfluoresceine diacetate succinimidyl ester (CFSE) at 37°C for 6 min to be used as targets in the ADCC assay. After washing 3 times with RPMI-1640 supplemented with 10% FCS, CFSE-labeled CMS5a or CMS5a/GITR cells were plated at various effector-to-target ratios with rat IgG or DTA-1 (2 μg/mL), incubated for 12 hrs, and analyzed by flow cytometry. For each sample, 20,000 non-CFSE labeled cells were collected, and the absolute number of CFSE-labeled surviving cells was counted. The survival percentage was calculated as the mean number of each of the three wells as follows: [(absolute number of surviving CFSE-labeled cells in control rat IgG-containing medium)−(absolute number of surviving CFSE-labeled cells in DTA-1-containing medium)]×100/(absolute number of surviving CFSE-labeled cells in control rat IgG-containing medium).

Statistical analysis

The Mann-Whitney U test was used to compare data from two groups. When equality of variance was proven by Levine's test, data comparison between 2 groups was evaluated by Student's *t*-test. The Kruskal-Wallis ANOVA test was used to compare data from four groups. *p*-values below 0.05 were considered statistically significant. Calculations were performed using SPSS Statistics v21.0 software (IBM).

Results

Effective inhibition of tumor growth by local treatment of HF10 combined with DTA-1

Since the therapeutic efficacy of the adjuvants included in immune-targeting Abs has been widely shown in the treatment of cancer, we hypothesized that the use of DTA-1, as an enhancer of tumor-specific $CD8^+$ T cell responses [26,27] in HF10 virotherapy might produce a satisfactory treatment outcome. To investigate this hypothesis, we used human NY-ESO-1 gene-transfected CT26 tumor cells (CT26/NY-ESO-1) for *in vitro* and *in vivo* studies as an H-$2D^d$-restricted murine CTL epitope of NY-ESO-1 had been identified in our laboratory [31]. Subcutaneously inoculated CT26/NY-ESO-1 tumors were treated by i.t. administration of HF10 with or without DTA-1 (Fig. 1A). Groups treated with either HF10 or DTA-1 showed weak suppression of tumor growth compared with the untreated group (control), and 2 out of 13 mice (15.4%) or 3 out of 19 mice (15.8%) showed

Table 1. Increase in the number of tumor-regressed mice by HF10 therapy combined with DTA-1.

Treatment	Number of complete tumor-regressed mice*/Number of treated mice (%)	
	CT26/NY-ESO-1	CMS5a
Cont. IgG	0/10 (0.0%)	0/13 (0.0%)
DTA-1	2/13 (15.4%)	0/13 (0.0%)
HF10	3/19 (15.8%)	0/13 (0.0%)
HF10+DTA-1	12/20 (60.0%)	3/13 (23.1%)

* Number of complete tumor-regressed mice was counted at 42 or 25 days after subcutaneous inoculation of CT26/NY-ESO-1 or CMS5a tumor cells, respectively.
doi:10.1371/journal.pone.0104669.t001

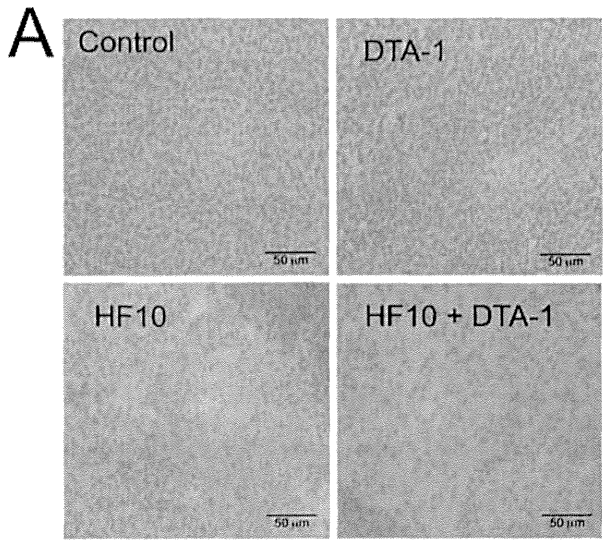
A
Control
DTA-1
HF10
HF10 + DTA-1
50 μm

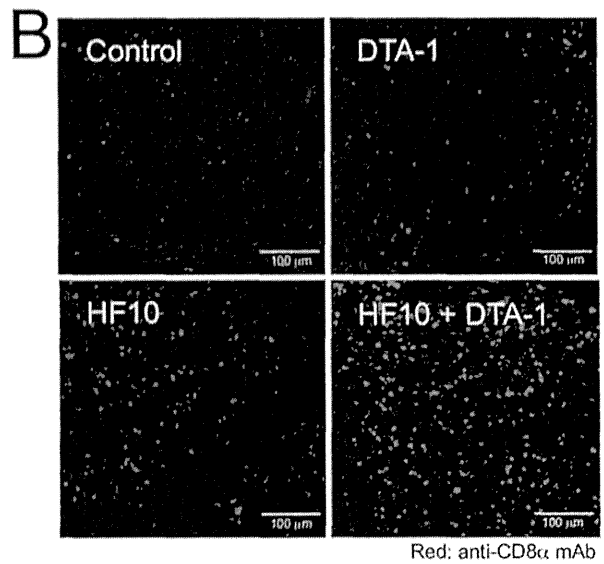
B
Control
DTA-1
HF10
HF10 + DTA-1
100 μm
Red: anti-CD8α mAb

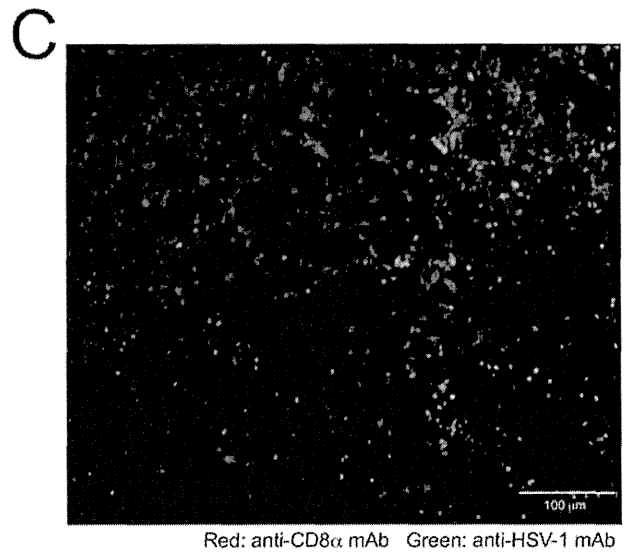
C
100 μm
Red: anti-CD8α mAb Green: anti-HSV-1 mAb

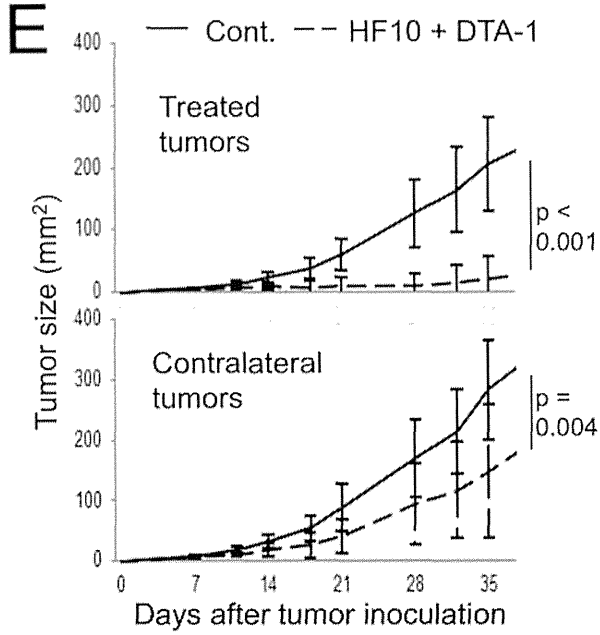
E
Cont.
HF10 + DTA-1
Treated tumors
Contralateral tumors
p < 0.001
p = 0.004
Tumor size (mm2)
Days after tumor inoculation

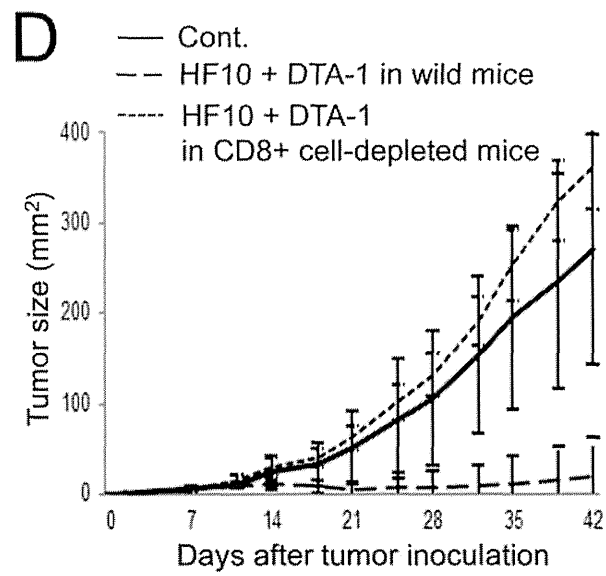
D
Cont.
HF10 + DTA-1 in wild mice
HF10 + DTA-1
in CD8+ cell-depleted mice
Tumor size (mm2)
Days after tumor inoculation

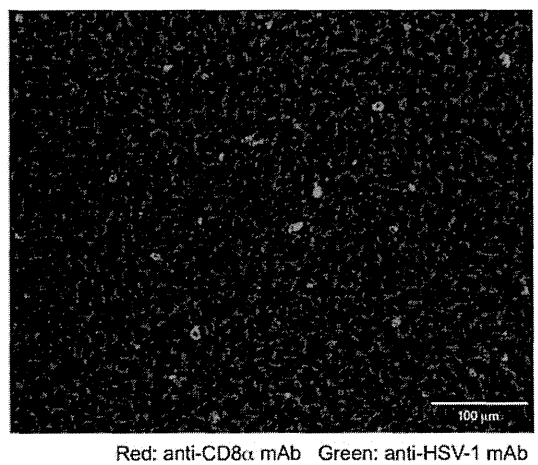
F
100 μm
Red: anti-CD8α mAb Green: anti-HSV-1 mAb

Figure 2. Kinetics of $CD8^+$ T cells after the combination therapy with HF10 and DTA-1. CT26/NY-ESO-1 tumor sections from untreated mice (control) or mice injected i.t. with DTA-1, HF10, or HF10 combined with DTA-1 were stained with hematoxylin and eosin (A), and phycoerythrin (PE)-conjugated anti-CD8α mAb and DAPI (B). (C) Frozen sections of CT26/NY-ESO-1 tumors from mice i.t. injected with HF10 combined with DTA-1 were stained with a PE-anti-CD8α monoclonal antibody, a fluorescein isothiocyanate (FITC)-anti-HSV-1 polyclonal antibody, and DAPI. (D) CT26/NY-ESO-1 growth (mm^2) in both i.t. HF10- and DTA-1-treated control or $CD8^+$ cell-depleted mice was measured. Seven mice per group were used. (E) Bilateral CT26/NY-ESO-1-bearing mice were treated with a combination of HF10 and DTA-1 in the tumors on the right flanks. Subsequent tumor growth (mm^2) of the treated right and contralateral left sites was measured. Tumor growth in untreated mice was measured and used as a control. Fourteen mice per group were used. By the Kruskal-Wallis ANOVA test, CT26/NY-ESO-1 growth inhibition by the combined HF10 and DTA-1 treatment in contralateral as well as treated sites was significantly different from the untreated control group. (F) CT26/NY-ESO-1 tumors from one side of bilateral tumor-bearing mice were treated i.t. with HF10 combined with DTA-1. Frozen sections of contralateral CT26/NY-ESO-1 tumors were stained with a PE-anti-CD8α monoclonal antibody, a fluorescein isothiocyanate (FITC)-anti-HSV-1 polyclonal antibody, and DAPI.
doi:10.1371/journal.pone.0104669.g002

complete tumor regression at 42 days after tumor inoculation, respectively (Table 1). In contrast, all mice in the group treated with both HF10 and DTA-1 showed statistically significant attenuation of tumor growth compared with the control group [$p<0.001$, Fig. 1A; complete tumor regression rate at 42 days: 60.0% (12 to 20 mice); Table 1]. In addition, CMS5a tumor growth in the group treated with both HF10 and DTA-1 was also suppressed significantly compared with the control or DTA-1-treated groups (Fig. 1B and Table 1).

We observed CT26/NY-ESO-1-regressed mice in another experiment for 2 months after HF10 and DTA-1 treatment. Tumor recurrence could not be seen in the tumor-regressed mice. In addition, these mice exhibited the resistance in tumor re-challenging.

$CD8^+$ T cells act as tumoricidal effectors in the combination therapy of HF10 with DTA-1

Intratumoral injection of HF10 resulted in the collapse of tumor structure with a decrease in the nuclear density of tumor cells, as shown at 7 days after the last HF10 treatment in both the group treated with HF10 and that treated with HF10 and DTA-1 (Fig. 2A). Tumor-infiltrating $CD8^+$ T cells were shown to be the most frequent population after the administration of HF10 combined with DTA-1 at 3 days after the final treatment (Fig. 2B). Importantly, these cells appeared to accumulate near HF10-infected tumor areas (Fig. 2C and S1A), suggesting that HF10 infection is able to attract $CD8^+$ T cells by leaking virus-associated proteins and tumor antigenic proteins from infected tumor cells and changing the tumor microenvironment after oncolysis. Inhibition of CT26/NY-ESO-1 growth by the combination therapy was completely negated by depleting $CD8^+$ cells by intravenous treatment with a murine CD8α-specific mAb (Fig. 2D), indicating that the tumor-infiltrating $CD8^+$ T cells shown in Figure 2B and 2C include tumoricidal effector populations. In the study using bilateral tumor-bearing mice, tumor growth inhibition by HF10 combined with DTA-1 occurred not only in the treated tumors but also in the contralateral non-treated tumors (Fig. 2E and S1B). In addition, the sections of contralateral tumor showed infiltrating $CD8^+$ T cells without HF10 infection (Fig. 2F and S1C). These results indicate that $CD8^+$ T cells activated in a local tumor site under the influence of HF10 and DTA-1 participate in systemic surveillance and could attack distant tumors without tissue destruction due to HF10 infection.

Augmentation of tumor-specific $CD8^+$ T cell responses by DTA-1 treatment in HF10 therapy

Next, we investigated whether the tumor- or HF10-specific $CD8^+$ T cell response was enhanced in CT26/NY-ESO-1-bearing mice by i.t. treatment with DTA-1 alone or HF10 combined with DTA-1. To detect low proportions of $CD8^+$ T cells with tumor specificity, spleen cells from tumor-regressed mice selected after i.t. treatment with DTA-1 at the indicated doses were stimulated with a CT26-specific AH-1 peptide or an NY-ESO-1 81–88 peptide to expand each population of peptide-specific $CD8^+$ T cells. As shown in Figure 3A, the response of CT26-specific IFN-γ-producing $CD8^+$ T cells was enhanced by DTA-1 in a dose-dependent manner. In addition, $CD8^+$ T cells with NY-ESO-1 specificity were observed when DTA-1 was administered at a high dose (10 μg). In this experiment, we used tumor-regressed mice because we could not enhance the negligible CT26-specific IFN-γ-producing $CD8^+$ T cell responses seen in tumor-bearers in a DTA-1 dose-dependent manner. Although CT26/NY-ESO-1 growth after i.t. treatment with DTA-1 was suppressed compared with the control group, tumor size was not different in each group of DTA-1 (0.5, 2.0, or 10.0 μg/mouse). Furthermore, HF10-specific $CD8^+$ T cells were found in addition to the AH-1-specific population (Fig. 3B left) when splenocytes from both HF10- and DTA-1-treated CT26/NY-ESO-1-bearing mice with HF10-infected CMS5a cells were cultured (Fig. 3B right). These results indicated that i.t. treatment of HF10 and DTA-1 had the capacity to enhance tumor- and HF10-specific $CD8^+$ T cell populations.

Disappearance of tumor-infiltrating $Foxp3^+$ cells after the treatment with DTA-1 in HF10 therapy

We hypothesized that the increase in tumor-specific $CD8^+$ T cell responses after DTA-1 treatment combined with HF10 therapy was involved in the attenuation and/or depletion of immune suppressors including Treg cells. To address this issue, CT26/NY-ESO-1 tumors obtained after DTA-1 treatment with or without HF10 were evaluated by immunohistological staining of tissue sections and flow cytometric analysis of infiltrating lymphocytes using a Foxp3-specific mAb. $Foxp3^+$ cells accumulated abundantly in both untreated and HF10-treated tumors, whereas a vigorous decrease in the number of Treg cells was shown in tumors following treatment with DTA-1 alone or DTA-1 combined with HF10 (Fig. 4A). This result was confirmed by flow cytometric analysis of tumor-infiltrating Treg cells. The frequency of tumoral $CD4^+$ $Foxp3^+$ Treg cells from the HF10- and DTA-1-treated group was decreased significantly compared with that from the untreated (control) group but not from the HF10- or DTA-1-treated mice (Fig. 4B). The decrease in the frequency of $Foxp3^+$ cells in the HF10-treated group (Fig. 4B) is possibly correlated with the decrease in tumor size due to HF10 treatment. This may be attributed to the lack of modulation of the absolute number of $Foxp3^+$ cells in the HF10-treated group unlike in the control group (Fig. 4A). DTA-1 is a rat IgG2b class mAb. By visualizing DTA-1 with the FITC-conjugated anti-rat IgG2b mAb, it was demonstrated that the tumor-infiltrating $CD4^+$ $Foxp3^+$ Treg population bound predominantly with DTA-1 at 6 hrs after i.t. injection (Fig. 4C), in parallel with the disappearance of tumoral Treg cells after treatment with DTA-1. Taken together, these results strongly indicate that DTA-1 was essential to the decrease in the number of $CD4^+$ $Foxp3^+$ cells.

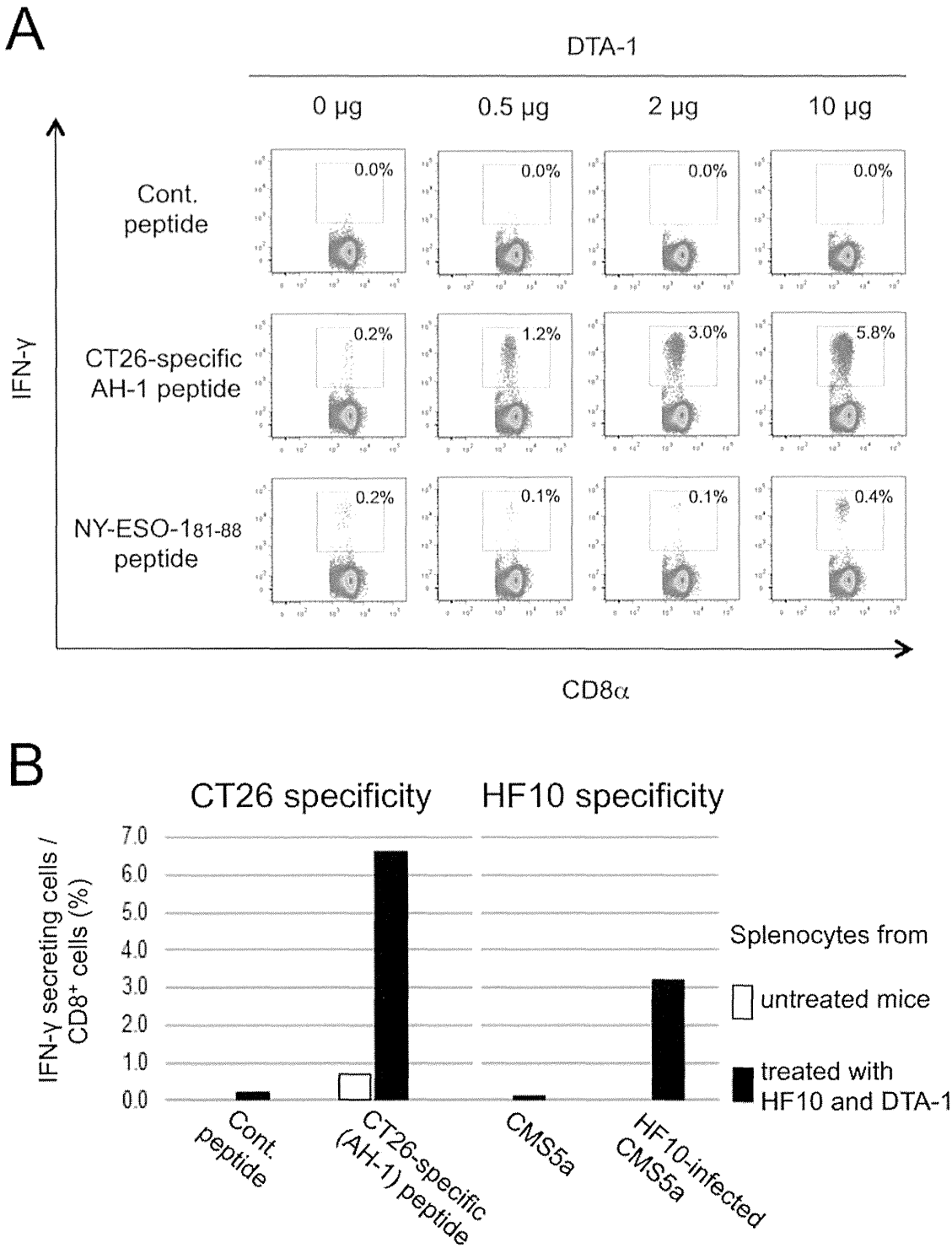

Figure 3. Generation of tumor- and HF10-specific CD8$^+$ T cells by intratumoral treatment of DTA-1 and HF10 combined with DTA-1. (A) CT26- and NY-ESO-1-specific CD8$^+$ T cell responses in CT26/NY-ESO-1-regressed mice by i.t. treatment of DTA-1 at indicated doses were assessed by intracellular staining of IFN-γ in splenocytes cultured with 10 μg/mL of the indicated peptides for 5 hrs. Splenocytes from two mice per group were pooled and assessed. (B) Splenocytes from untreated and both i.t. HF10- and DTA-1-treated CT26/NY-ESO-1-bearing mice were obtained at 5 days after final treatment, and cultured with AH-1 peptide (10 μg/mL) or HF10-infected CMS5a tumor cells for 5 hrs. Splenocytes from ten mice per group were pooled and assessed. The obtained cells were immunohistologically stained for intracellular IFN-γ. The 9 m peptide and uninfected CMS5a cells were used as controls.
doi:10.1371/journal.pone.0104669.g003

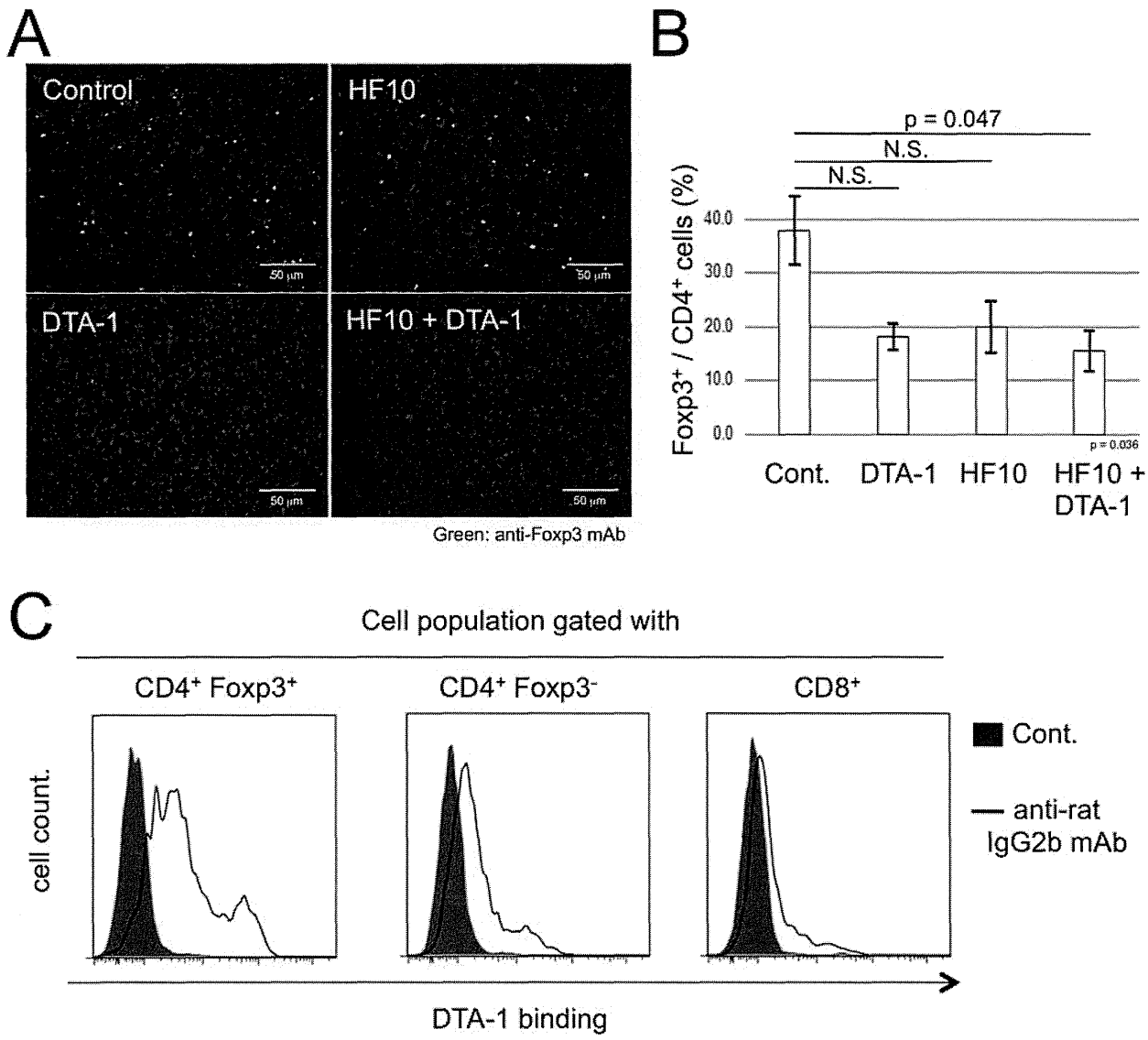

Figure 4. Disappearance of DTA-1-conjugated tumor-infiltrating CD4$^+$ Foxp3$^+$ cells after combined i.t. treatment with HF10 and DTA-1. (A) CT26/NY-ESO-1 tumor sections form untreated group (control) or group from mice injected i.t. with DTA-1, HF10, or HF10 combined with DTA-1 were stained with FITC-anti-Foxp3 mAb and DAPI. (B) The frequency of tumor-infiltrating CD4$^+$ Foxp3$^+$ Treg cells from mice injected i.t. with HF10, DTA-1, or HF10 combined with DTA-1 at 12 days after CT26/NY-ESO-1 inoculation was assessed by flow cytometry. Data from 4 individual experiments were analyzed statistically. Kruskal-Wallis ANOVA test was used to compare data from the 4 groups. The decrease in the frequency of tumoral CD4$^+$ Foxp3$^+$ Treg cells in the HF10 and DTA-1 combined treatment group was significantly different from untreated control, but not from the HF10- or DTA-1-treated group (N.S: Not significant). (C) At 6 hrs after DTA-1 injection into day 9 CT26/NY-ESO-1 tumors, tumor-infiltrating cells collected under collagenase-free conditions were analyzed by flow cytometry after staining with FITC-labeled anti-rat IgG2b mAb to detect DTA-1-bound cells.
doi:10.1371/journal.pone.0104669.g004

Depletion of tumor-infiltrating Treg cells by DTA-1-mediated cellular cytotoxicity

Fluorescent immunohistological studies using double labeling with anti-rat IgG2b mAb (for DTA-1) and F4/80- (for macrophages) or Foxp3- (for Tregs) specific mAbs were performed to determine the mechanisms of DTA-1-dependent depletion of CT26/NY-ESO-1 tumor-infiltrating Treg cells. At 6 hrs after DTA-1 treatment, Foxp3$^+$ cells clustered at the DTA-1-stained peritumor sites, whereas Foxp3$^+$ cells did not accumulate in the control rat IgG-treated case (Fig. 5A and S2A). Images of red fluorescence from DTA-1 or the control rat IgG merged with the green fluorescence from F4/80$^+$ macrophages in nearby tumor stroma (Fig. 5B; C1, D1, and S2B) indicated that DTA-1 and rat IgG bound with macrophage-expressing FcRs. In addition, a large number of cells visualized in lymphocyte-like formation by staining with anti-rat IgG2b mAb were positive for Foxp3 (Fig. 5B; D2, D3; Fig. S3A and B) and were in contact with macrophages in various areas of DTA-1–treated tumors (Fig. 5B; D2; Fig. S3A). These results strongly support the hypothesis that DTA-1

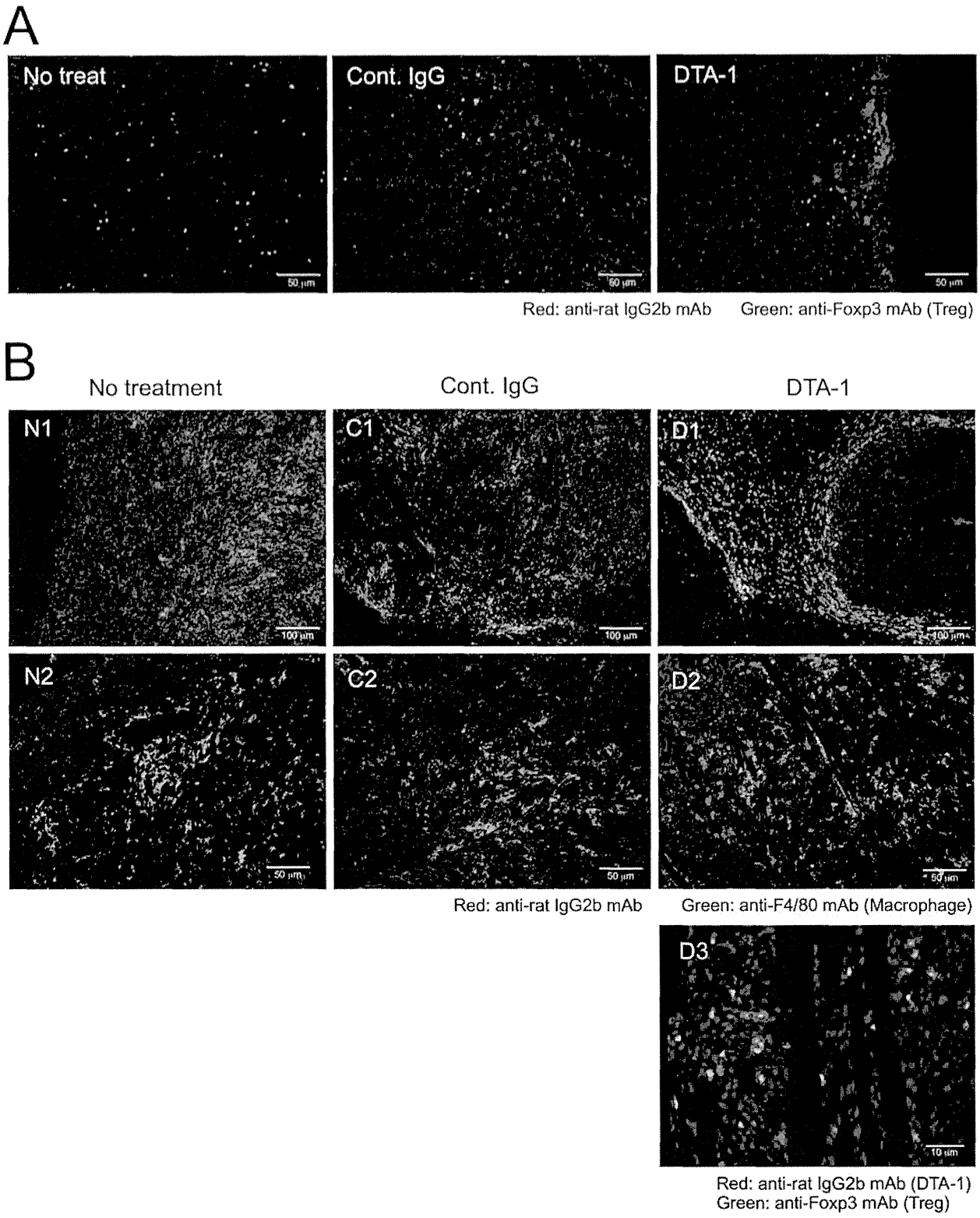

Figure 5. Kinetics of Foxp3$^+$ Treg cells and F4/80$^+$ macrophages in DTA-1-treated tumors. Frozen sections of CT26/NY-ESO-1 tumors obtained at 6 hrs after DTA-1 i.t. injection were stained with FITC-conjugated anti-Foxp3 mAb, PE-conjugated anti-rat IgG2b mAbs and DAPI (A and B: D3), or FITC-anti-F4/80 mAb, PE-anti-rat IgG2b mAb, and DAPI (B: D1 and D2). Sections from untreated and control rat IgG-treated tumors were used as controls (A and B: N1, N2, C1, C2). Representative photos from three experiments are shown.
doi:10.1371/journal.pone.0104669.g005

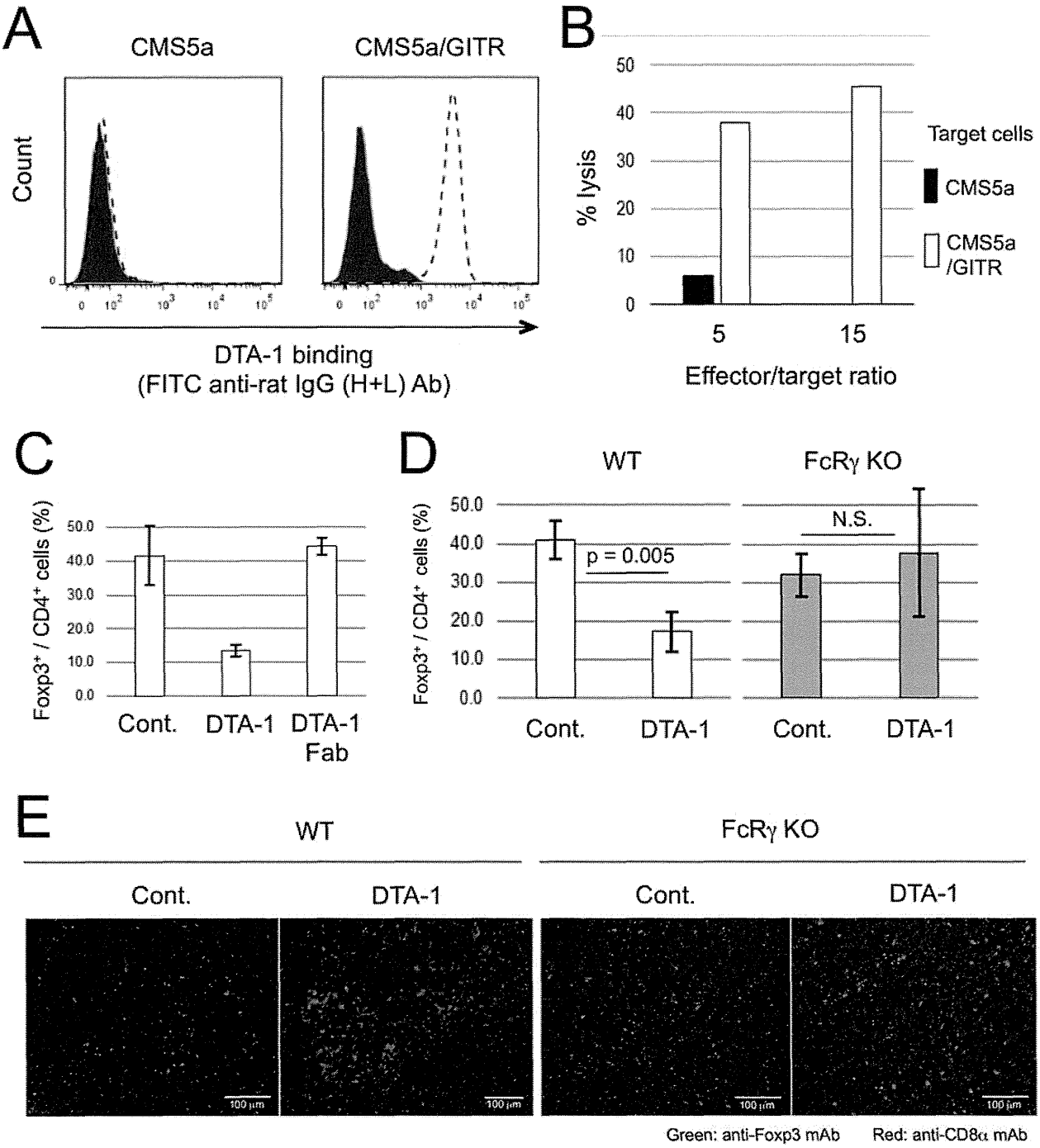

Figure 6. DTA-1-mediated depletion of tumor-infiltrating CD4$^+$ Foxp3$^+$ Treg cells by ADCC. (A) DTA-1- (dotted line) or isotype control (solid line)-treated CMS5a and murine GITR gene-transfected CMS5a (CMS5a/GITR) cells were stained with a FITC-conjugated anti-rat IgG (H+L) antibody and analyzed by flow cytometry. (B) CFSE-labeled CMS5a and CMS5a/GITR cells were used as targets. The mixture of IFN-γ-activated RAW264.7 cells (effector cells) and target cells were incubated for 12 hrs with control IgG or DTA-1 at effector/target ratios of 5 and 15. (C) Frequency of Foxp3$^+$ cells in tumor-infiltrating CD4$^+$ cell population at 3 days after i.t. DTA-1 or Fc-digested DTA-1 (DTA-1 Fab) treatment was measured by flow cytometric analysis. (D) Frequency of Foxp3$^+$ cells in tumor-infiltrating CD4$^+$ cell population at 3 days after DTA-1 i.t. treatment in wild-type or FcRγ KO mice was measured by flow cytometric analysis. By Student's t-test, the decrease in the frequency of Foxp3$^+$ cells in DTA-1-treated CT26/NY-ESO-1 tumors of wild type mice, but not FcRγ KO mice (N.S.: Not significant), was significantly different from untreated control group. (E) Frozen sections of CT26/NY-ESO-1 tumors obtained at 3 days after DTA-1 i.t. treatment in wild type and FcRγ KO mice were stained with FITC-anti-Foxp3 and PE-anti-CD8α mAbs, and DAPI.
doi:10.1371/journal.pone.0104669.g006

participates in GITR$^+$ Foxp3$^+$ Treg depletion by ADCC at the treated tumor sites.

To examine whether DTA-1 can mediate ADCC in a murine system, we performed an *in vitro* ADCC assay using IFN-γ-activated RAW264.7 macrophage cells as an effector and murine GITR gene-transfected CMS5a (CMS5a/GITR) cells (Fig. 6A) as a target. CMS5a/GITR cells were lysed in the presence of DTA-1 in a GITR-specific manner (Fig. 6B). We further investigated *in vivo* the ADCC effects of DTA-1 using Fc portion-digested DTA-1 (DTA-1 Fab) and FcRγ KO mice. Depletion of CD4$^+$ Foxp3$^+$ Treg cells in CT26/NY-ESO-1 tumors was not observed following i.t. DTA-1 Fab treatment (Fig. 6C). In addition, no significant decreases in the number of CD4$^+$ Foxp3$^+$ Treg cells and accumulation of CD8$^+$ T cells were detected by DTA-1 treatment in FcRγ KO mice, unlike the results from wild-type mice (Fig. 6D, 6E, and S4). These results clearly indicated the direct participation of DTA-1 in Treg cell depletion by ADCC.

Taken together, these results show that HF10 virotherapy combined with DTA-1 elicits a powerful therapeutic effect against tumors via the accumulation of CD8$^+$ T cells, after tumor destruction by HF10 and the enhancement of tumor- and virus-specific CD8$^+$ T cell responses directly or indirectly by depletion of immune-suppressive Treg cells at tumor sites by DTA-1.

Discussion

Many studies involving oncolytic virus combined with systemic administration of cytotoxic agents have shown promising results in animal models. However, almost all of the studies have avoided the important issue of lymphocyte suppression caused by steroids as an antiemetic, implying the clinical inapplicability of such cytotoxic agents. Tumor therapy promises an era of safety in using noninvasive immunomodulatory agents including PD-1-, CTLA-4- and GITR-specific mAbs. Unfortunately, all of them have produced slight immune-related slight adverse events such as diarrhea, rashes or pruritis [35–38]. In addition, systemic administration of immunomodulators can elicit serious autoimmune diseases. A study from another group has shown that in a murine model, treatment with 50 μg/mouse DTA-1 induces antitumor activity and weak autoimmune reactions [39]. In this study, we also demonstrated that HF10 virotherapy combined with a GITR-targeting mAb in local tumor sites at more clinical appropriate lower and safer doses, elicits tumor lysis by augmented systemic tumor-specific CD8$^+$ T cell activity with negligible toxicity. Therefore, local treatment of immunomodulators is a promising method for the future treatment of tumors.

The use of blocking Abs for suppressing immune signals has shown clinical benefits in the treatment of solid tumors [40–42]. Both PD-1 and CTLA-4, which are expressed on activated T cell surfaces, inhibit tumoricidal effector T cell responses by engagement via specific ligands that are expressed on various tumor cells [23]. However, high densities of tumor-infiltrating CD4$^+$ CD25$^+$ Foxp3$^+$ Treg cells have been correlated with poor survival [43–45]. Treg cells express both PD-1 and CTLA-4 in the steady state without activation. PD-1 and CTLA-4 signals result in Treg induction and maintenance, and subsequent outbreak of autoimmune diseases [46]. Interestingly, it has been reported that an anti-CTLA-4 antibody augments tumoricidal effector T cells by downregulation of Treg cell functions, including ADCC-mediated depletion of Treg cells [47], which is similar to our GITR-targeting results. These reports indicate that the blockade of immune checkpoint molecules involves the activation of tumoricidal effector T cells by preventing interactions with specific ligands on tumor cells and inhibiting Treg cell functions.

The expression of GITR has been observed on CD4$^+$ CD25$^+$ Treg cells at relatively high levels [24,25], which is consistent with our results. In addition, the GITR-GITRL interaction has been known to attenuate Treg cell function via the loss of Foxp3 expression as well as enhance tumor-specific effector CD4$^+$ and CD8$^+$ T cell functions [27,39,48,49]. In this study, we demonstrated the use of DTA-1 as a depletion antibody because Fc-digested DTA-1 and intact DTA-1 in FcRγ KO mice did not participate in the downregulation of Foxp3 expression. After i.t. DTA-1 injection, macrophages appeared to attract DTA-1-conjugated Treg cells via their FcR and migrate to peritumor sites, as shown in Fig. 5, and the results suggest that the peritumoral stroma is a crucial place for ADCC triggering. Since CCL22 secreted by macrophages is known to be a chemoattractant for Treg cells [43,50], such chemokines might participate in DTA-1-mediated Treg cell depletion. Further studies are necessary to elucidate the molecular mechanisms of tumoral ADCC.

As indicated in Fig. 4C, a small proportion of tumor-infiltrating CD8$^+$ T cells bound with i.t. treated DTA-1. In addition, DTA-1 enhanced tumor-specific CD8$^+$ T cell responses in a dose-dependent manner in tumor-regressed mice as shown in Fig. 3. These results suggest that DTA-1 acts as a direct activator of CD8$^+$ T cells, although we could not rule out the possibility that tumor-specific CD8$^+$ T cell responses were increased by DTA-1 dose-dependent depletion of immune suppressive Treg cells. Indeed, it has been reported that the function and activity of CTLs are augmented by the signals through GITR [26,48,51]. In this study, HF10-specific CD8$^+$ T cells were detected after both HF10 and DTA-1 injections, concomitant with vigorous tumor-specific CTL responses. La et al. have reported that DTA-1 elicits immediately explosive HSV-1-specific CD8$^+$ CTL and CD4$^+$ Th responses in HSV-1-infected mice [52]. In addition, we found in this study that DTA-1 was detected in tumor-draining lymph nodes soon after i.t. injection (Fig. S5), suggesting the relationship between DTA-1 and quick generation of tumor-specific CTLs. Thus, it is likely that HF10-specific CTL responses induced by DTA-1 change the tumor microenvironment to facilitate the expansion of CTLs in tumor-draining lymph nodes.

In conclusion, local HF10 therapy combined with DTA-1 should be suitable for the treatment of cancer patients without crucial side effects. The benefits of the combined treatment regimen include the vigorous expansion of tumoricidal CTLs associated with the early HF10-specific CTL responses, inhibition of tumor formation by HF10 infection, direct expansion of CD8$^+$ T cells by DTA-1, and negation of immune suppressive Treg cell activities by DTA-1-mediated ADCC and/or DTA-1 signaling.

Supporting Information

Figure S1 Systemic surveillance of tumoricidal CTLs after HF10 combination therapy with DTA-1 at local tumor sites. (A) The images of red (PE), green (FITC), and blue (DAPI) fluorescence that were merged to produce Fig. 2C. (B) Bilateral CT26/NY-ESO-1-bearing mice were treated i.t. with a combination of HF10 and DTA-1 in tumors on the right flanks of mice. Tumor growth in the treated right and contralateral left sites was measured. Photos show representative mice at 25 days after CT26/NY-ESO-1 inoculation from the control and dual HF10- and DTA-1-treated groups. (C) The three images of red (PE), green (FITC), and blue (DAPI) fluorescence that were merged to produce Fig. 2F.
(TIF)

Figure S2 The three fluorescence components of the merged images of Fig. 5A and Fig. 5B (N1, C1, and D1).

Three separate images of red (PE), green (FITC), and blue (DAPI) fluorescence that were merged to produce Fig. 5A (A) and N1, C1, and D1 of Fig. 5B (B).
(TIF)

Figure S3 The three fluorescence components of the merged images of N2, C2, D2, and D3 in Fig. 5B. The three separate images of red (PE), green (FITC), and blue (DAPI) fluorescence that were merged to produce N2, C2, D2, and D3 images in Fig. 5B.
(TIF)

Figure S4 The three fluorescence components of the merged images in Fig. 6E. The three separate images of red (PE), green (FITC), and blue (DAPI) fluorescence that were merged to produce Fig. 6E.
(TIF)

Figure S5 Drafting of i.t. treated DTA-1 into tumor-draining lymph nodes. Frozen sections of tumor-draining lymph nodes obtained at 6 hrs after intratumoral DTA-1 or DTA-1 Fab treatment were stained with a FITC-conjugated anti-rat IgG2b antibody, a phycoerythrin (PE)-conjugated anti-F4/80 antibody, and DAPI.
(TIF)

Acknowledgments

We thank Drs. N. Harada, Y. Miyahara, T. Kato, and T. Takahashi for helpful discussions, and M. Yamane for technical assistance.

Author Contributions

Conceived and designed the experiments: MI NS HS. Performed the experiments: MI NS. Analyzed the data: MI NS DM HI HS. Contributed reagents/materials/analysis tools: J. Mitsui MT J. Mineno. Contributed to the writing of the manuscript: MI NS.

References

1. Vaha-Koskela MJ, Heikkila JE, Hinkkanen AE (2007) Oncolytic viruses in cancer therapy. Cancer Lett 254: 178–216.
2. Breitbach CJ, Reid T, Burke J, Bell JC, Kirn DH (2010) Navigating the clinical development landscape for oncolytic viruses and other cancer therapeutics: no shortcuts on the road to approval. Cytokine Growth Factor Rev 21: 85–89.
3. Eager RM, Nemunaitis J (2011) Clinical development directions in oncolytic viral therapy. Cancer Gene Ther 18: 305–317.
4. Kim JH, Oh JY, Park BH, Lee DE, Kim JS, et al. (2006) Systemic armed oncolytic and immunologic therapy for cancer with JX-594, a targeted poxvirus expressing GM-CSF. Mol Ther 14: 361–370.
5. Park BH, Hwang T, Liu TC, Sze DY, Kim JS, et al. (2008) Use of a targeted oncolytic poxvirus, JX-594, in patients with refractory primary or metastatic liver cancer: a phase I trial. Lancet Oncol 9: 533–542.
6. Merrick AE, Ilett EJ, Melcher AA (2009) JX-594, a targeted oncolytic poxvirus for the treatment of cancer. Curr Opin Investig Drugs 10: 1372–1382.
7. Hwang TH, Moon A, Burke J, Ribas A, Stephenson J, et al. (2011) A mechanistic proof-of-concept clinical trial with JX-594, a targeted multi-mechanistic oncolytic poxvirus, in patients with metastatic melanoma. Molecular Ther 19: 1913–1922.
8. Breitbach CJ, Burke J, Jonker D, Stephenson J, Haas AR, et al. (2011) Intravenous delivery of a multi-mechanistic cancer-targeted oncolytic poxvirus in humans. Nature 477: 99–102.
9. Liu BL, Robinson M, Han ZQ, Branston RH, English C, et al. (2003) ICP34.5 deleted herpes simplex virus with enhanced oncolytic, immune stimulating, and anti-tumour properties. Gene Ther 10: 292–303.
10. Kaufman HL, Kim DW, DeRaffele G, Mitcham J, Coffin RS, et al. (2010) Local and distant immunity induced by intralesional vaccination with an oncolytic herpes virus encoding GM-CSF in patients with stage IIIc and IV melanoma. Ann Surg Oncol 17: 718–730.
11. Kaufman HL, Bines SD (2010) OPTIM trial: a Phase III trial of an oncolytic herpes virus encoding GM-CSF for unresectable stage III or IV melanoma. Future Oncol 6: 941–949.
12. Andtbacka RHI, Collichio FA, Amatruda T, Senzer NN, Chesney J, et al. (2013) OPTiM: A randomized phase III trial of talimogene laherparepvec (T-VEC) versus subcutaneous (SC) granulocyte-macrophage colony-stimulating factor (GM-CSF) for the treatment (tx) of unresected stage IIIB/C and IV melanoma. J Clin Oncol 31: suppl; abstr LBA9008.
13. Campadelli-Fiume G, De Giovanni C, Gatta V, Nanni P, Lollini PL, et al. (2011) Rethinking herpes simplex virus: the way to oncolytic agents. Rev Med Virol 21: 213–226.
14. Nishiyama Y, Kimura H, Daikoku T (1991) Complementary lethal invasion of the central nervous system by nonneuroinvasive herpes simplex virus types 1 and 2. J Virol 65: 4520–4524.
15. Mori I, Liu B, Goshima F, Ito H, Koide N, et al. (2005) HF10, an attenuated herpes simplex virus (HSV) type 1 clone, lacks neuroinvasiveness and protects mice against lethal challenge with HSV types 1 and 2. Microbes Infect 7: 1492–1500.
16. Nakao A, Kimata H, Imai T, Kikumori T, Teshigahara O, et al. (2004) Intratumoral injection of herpes simplex virus HF10 in recurrent breast cancer. Ann Oncol 15: 988–989.
17. Fujimoto Y, Mizuno T, Sugiura S, Goshima F, Kohno S, et al. (2006) Intratumoral injection of herpes simplex virus HF10 in recurrent head and neck squamous cell carcinoma. Acta Otolaryngol 126: 1115–1117.
18. Kimata H, Imai T, Kikumori T, Teshigahara O, Nagasaka T, et al. (2006) Pilot study of oncolytic viral therapy using mutant herpes simplex virus (HF10) against recurrent metastatic breast cancer. Ann Surgical Oncol 13: 1078–1084.
19. Nakao A, Kasuya H, Sahin TT, Nomura N, Kanzaki A, et al. (2011) A phase I dose-escalation clinical trial of intraoperative direct intratumoral injection of HF10 oncolytic virus in non-resectable patients with advanced pancreatic cancer. Cancer Gene Ther 18: 167–175.
20. Kohno SI, Luo C, Nawa A, Fujimoto Y, Watanabe D, et al. (2007) Oncolytic virotherapy with an HSV amplicon vector expressing granulocyte-macrophage colony-stimulating factor using the replication-competent HSV type 1 mutant HF10 as a helper virus. Cancer Gene Ther 14: 918–926.
21. Goshima F, Esaki S, Luo C, Kamakura M, Kimura H, et al. (2014) Oncolytic viral therapy with a combination of HF10, a herpes simplex virus type 1 variant and granulocyte-macrophage colony-stimulating factor for murine ovarian cancer. Int J Cancer 134: 2865–2877.
22. Nocentini G, Giunchi L, Ronchetti S, Krausz LT, Bartoli A, et al. (1997) A new member of the tumor necrosis factor/nerve growth factor receptor family inhibits T cell receptor-induced apoptosis. Proc Natl Acad Sci USA 94: 6216–6221.
23. Pardoll DM (2012) The blockade of immune checkpoints in cancer immunotherapy. Nat Rev Cancer 12: 252–264.
24. McHugh RS, Whitters MJ, Piccirillo CA, Young DA, Shevach EM, et al. (2002) CD4(+)CD25(+) immunoregulatory T cells: gene expression analysis reveals a functional role for the glucocorticoid-induced TNF receptor. Immunity 16: 311–323.
25. Shimizu J, Yamazaki S, Takahashi T, Ishida Y, Sakaguchi S (2002) Stimulation of CD25(+)CD4(+) regulatory T cells through GITR breaks immunological self-tolerance. Nat Immunol 3: 135–142.
26. Cote AL, Zhang P, O'Sullivan JA, Jacobs VL, Clemis CR, et al. (2011) Stimulation of the glucocorticoid-induced TNF receptor family-related receptor on CD8 T cells induces protective and high-avidity T cell responses to tumor-specific antigens. J Immunol 186: 275–283.
27. Nishikawa H, Kato T, Hirayama M, Orito Y, Sato E, et al. (2008) Regulatory T cell-resistant CD8+ T cells induced by glucocorticoid-induced tumor necrosis factor receptor signaling. Cancer Res 68: 5948–5954.
28. Rosenzweig M, Ponte J, Apostolou I, Doty D, Guild J, et al. (2010) Development of TRX518, an aglycosyl humanized monoclonal antibody (Mab) agonist of huGITR. J Clin Oncol 28: suppl; abstr e13028.
29. Takai T, Li M, Sylvestre D, Clynes R, Ravetch JV (1994) FcR gamma chain deletion results in pleiotrophic effector cell defects. Cell 76: 519–529.
30. Lerner WA, Pearlstein E, Ambrogio C, Karpatkin S (1983) A new mechanism for tumor induced platelet aggregation. Comparison with mechanisms shared by other tumor with possible pharmacologic strategy toward prevention of metastases. Int J Cancer 31: 463–469.
31. Muraoka D, Kato T, Wang L, Maeda Y, Noguchi T, et al. (2010) Peptide vaccine induces enhanced tumor growth associated with apoptosis induction in CD8+ T cells. J Immunol 185: 3768–3776.
32. Ikeda H, Ohta N, Furukawa K, Miyazaki H, Wang L, et al. (1997) Mutated mitogen-activated protein kinase: a tumor rejection antigen of mouse sarcoma. Proc Natl Acad Sci USA 94: 6375–6379.
33. Huang AY, Gulden PH, Woods AS, Thomas MC, Tong CD, et al. (1996) The immunodominant major histocompatibility complex class I-restricted antigen of a murine colon tumor derives from an endogenous retroviral gene product. Proc Natl Acad Sci USA 93: 9730–9735.
34. Mitsui J, Nishikawa H, Muraoka D, Wang L, Noguchi T, et al. (2010) Two distinct mechanisms of augmented antitumor activity by modulation of immunostimulatory/inhibitory signals. Clin Cancer Res 16: 2781–2791.